UNIVERSITY OF GAZİANTEP

GRADUATE SCHOOL OF

NATURAL & APPLIED SCIENCES

EXPERIMENTAL STUDY ON OPTIMISATION OF CUTTING PARAMETERS IN ABRASIVE WATERJET MACHINE

M. Sc. THESIS

IN

MECHANICAL ENGINEERING

BY

HAKAN ÇANDAR

JULY 2012

Experimental Study on Optimisation of Cutting Parameters in Abrasive Waterjet Machine

M. Sc. Thesis

in

Mechanical Engineering

University of Gaziantep

Supervisor

Prof. Dr. İ. Hüseyin Filiz

By

Hakan Çandar

July – 2012

Name of the thesis: Experimental Study on Optimisation of Cutting Parameters in Abrasive Waterjet Machine.

Name of the student: Hakan ÇANDAR

Exam date: 19.07.2012

Approval of the Graduate School of Natural & Applied Sciences
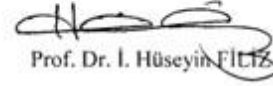
Prof. Dr. Ramazan KOÇ

Director

I certify that this thesis satisfies all the requirements as a thesis for the degree of Master of Science

Prof. Dr. L. Canan DÜLGER

Head of Department

This is to certify that we have read this thesis and that in our opinion it is fully adequate, in scope and quality, as a thesis for the degree of Master of Science

Prof. Dr. İ. Hüseyin FİLİZ

Supervisor

Examining Committee Members   Signature
Title and Name-surname

1. Prof. Dr. İ. Hüseyin FİLİZ

2. Prof. Dr. Ömer EYERCİOĞLU

3. Prof. Dr. İ. Halil GÜZELBEY

4. Prof. Dr. Türkay DERELİ

5. Doç. Dr. Oğuzhan YILMAZ

iii

I declared that the related thesis is written properly according to academic and ethic rules and using all literature information referenced in the related thesis.

Name and Surname

Signature

ABSTRACT

EXPERIMENTAL STUDY ON OPTIMISATION OF CUTTING PARAMETERS IN ABRASIVE WATERJET MACHINE

ÇANDAR, Hakan

M.Sc. in Mechanical Eng.

Supervisor: Prof. Dr. İ. Hüseyin FİLİZ

JULY 2012, 67 pages

This work contains experimental analysis of metallic surfaces generated by abrasive waterjet (AWJ) machine for Al 7075 alloy which is often used as structural material in aerospace and automobile industries. Water pressure, traverse speed and stand-off distance are the three factors considered in most of the studies. In this study, thickness of the material is added as another factor and effects of these four parameters on cutting performance (surface roughness and kerf geometry) are investigated. For this purpose, a total of 81 cuts are performed according to three-level full factorial design of experiment method and results are discussed by drawing main effect and interaction effect plots. Empirical models for surface roughness and kerf taper angle are then established for the prediction and optimisation of AWJ performance by using artificial neural network (ANN) and response surface methodology (RSM). Finally, the models are compared to each other on the basis of commonly used statistical parameters.

Key Words: AWJ, surface roughness, kerf geometry, ANN, RSM

ÖZET

AŞINDIRICILI SU JETİ TEZGAHINDA KESME PARAMETRELERİNİN OPTİMİZASYONUNA YÖNELİK DENEYSEL ÇALIŞMA

ÇANDAR, Hakan

Yüksek Lisans Tezi, Makine Müh. Bölümü

Tez yöneticisi: Prof. Dr. İ. Hüseyin FİLİZ

Temmuz 2012, 67 sayfa

Bu çalışmada, aşındırıcılı su jeti (ASJ) kesme tezgahında kesme parametrelerinin yüzey kalitesi ve çentik geometrisi üzerine yapılan deneysel analizler sunulmuştur. Su basıncı, ilerleme hızı ve nozul-iş parçası arasındaki mesafe birçok çalışmada ele alınan faktörlerdir. Bu çalışmada, malzeme kalınlığı başka bir faktör olarak eklenmiş ve bu dört parametrenin kesme performansına (yüzey kalitesi ve çentik oluşumu) etkileri araştırılmıştır. Bu amaçla, havacılık ve otomobil endüstrisinde sıkça kullanılan Al 7075 alaşımının üç seviyeli tam faktöriyel deney tasarımı yöntemine göre toplam 81 adet kesimi gerçekleştirilmiştir. Daha sonra yapay sinir ağı (YSA) ve yüzey yanıt yöntemleri kullanılarak ASJ performansının tahmini ve optimizasyonu için ampirik modeller kurulmuştur. Son olarak bu modeller istatistiksel parametreler baz alınarak birbirleriyle kıyaslanmıştır.

Key Words: ASJ, yüzey pürüzlülüğü, çentik geometrisi, YSA, yüzey yanıt yöntemi.

ACKNOWLEDGEMENTS

TABLE OF CONTENT

LIST of FIGURES

LIST of TABLES

CHAPTER 1

INTRODUCTION

Abrasive waterjet cutting is a non-traditional cutting process that has being used in many industrial applications in the last two decades. The advantages offered by the abrasive waterjet such as no thermal distortion, high machining versatility and small cutting forces, make it well suited to compete and even replace many traditional and non-traditional cutting technologies [1]. Cutting operation is performed by a supersonic water jet containing abrasive particles and almost any types of materials have the thickness of over 100 mm can be cut by using this method [2].

Abrasive waterjet has been moving onto the scene since about 1980s as an improved type of waterjet that was first attempted by forestry engineer Norman Franz in 1950s. Today, it is highly used in aerospace, automotive and electronics industries. For example, titanium bodies for military aircrafts, engine components (aluminium, titanium, heat resistant alloys), aluminium body parts and interior cabin parts in aerospace industries, interior trim (head liners, trunk liners, door panels), fibre glass body components and bumpers in automotive industries, circuit boards and cable stripping in electronics industries are generally made by using this technology [3].

In abrasive waterjet machining there are various parameters influence the cutting quality which is measured by surface quality and kerf taper. These can be categorized as process and machine parameters. The first group includes water pressure, traverse speed (rectilinear speed while cutting), stand-off distance (the distance between the nozzle and the workpiece), abrasive type, abrasive grid size and abrasive flow rate. Orifice diameter, mixing tube diameter and length of mixing tube are considered as the parameters in the second group. Cutting quality is influenced by these parameters. Although process parameters are easily adjusted for each

different cutting condition, machine parameters are generally kept constant during the cutting operation.

There are many studies for the investigation of the effects of process parameters on the cutting quality. Some of them considered a set of process parameters while some others considered different set of parameters. Only few are available for the investigation of the effect of material thickness on the surface roughness and kerf geometry. In this work, effects of traverse speed, water pressure, stand-off distance and material thickness are investigated experimentally and predictive models for surface roughness and kerf taper have been suggested by using artificial neural network (ANN) and response surface methodology (RSM).

Topics covered in this thesis are literature survey, abrasive waterjet machine, material and method, modelling and discussion and conclusion. Literatures related to effects of cutting parameters on cutting quality and modelling with ANN and RSM methods are treated separately in chapter 2. Brief information about AWJ cutting machine is given in chapter 3. Experimental set-up and procedure are explained and experimental results are discussed in chapter 4. Finally, the results obtained in chapter 4 are used for generating mathematical models by using both ANN and RSM in chapter 5.

CHAPTER 2

LITERATURE SURVEY

2.1 INTRODUCTION

In AWJ cutting, the cutting quality is generally evaluated in terms of surface roughness and kerf taper. Studies have shown that these terms are directly based on the process parameters. Therefore, researchers are generally concentrated on the investigation of effects of these parameters. Also, in some of these studies, results have been combined with various modelling methods in order to estimate cutting quality without going through the experiments. This chapter includes brief summaries of previous studies. Reviews of studies related to effects of process parameters on surface roughness and kerf geometry are presented first. And then, the studies related to modelling methods (artificial neural network (ANN), response surface methodology (RSM)) are presented.

2.2 STUDIES ON EFFECTS OF CUTTING PARAMETERS ON SURFACE QUALITY AND KERF GEOMETRY

Wang and Wong [4] have investigated the relationships between kerf characteristics and process parameters for metallic coated sheet steels based on statistically designed experiment. In the experiment, three levels of water pressure, transverse speed, standoff distance and abrasive flow rate are selected as process parameters to investigate the effects of them into top width and bottom width, kerf taper, burr formation as well as surface roughness. For this aim, a total of 81 cuts are undertaken in three level four factor full factor design experiment. It is found that optimum water pressure, small standoff distance and low traverse speed should be used for increasing the cutting quality.

Külekci and Akkurt [5] have investigated the relationship between surface finish produced by abrasive waterjet and associated cutting process: water pressure, orifice diameter, the length of mixing tube, abrasive mesh size and traverse speed for aluminium, glass, steel and rubber specimens. In another study, Akkurt et al. [6] have studied on the effects of feed rate and thickness of workpiece on the surface roughness of pure aluminium, Al-061, brass-353, AISI 1030 and AISI 304 stainless steel. For this purpose, two levels of thickness values are selected with two different feed rates for each material. Experiments have illustrated that surface quality deteriorates when the depth of cut gets deeper and also thinner specimens show better surface quality.

Çaydaş and Hasçalık [7] have illustrated the effect of process parameters on surface roughness for AA 7075 Aluminium alloy. Taguchi's design of experiment is used for the purpose of reduction the number of the experiments. Based on the analysis of variance (ANOVA) and F-tests, water pressure is found as the most effective parameter, followed by traverse speed, abrasive flow rate and stand-off distance.

Karakurt et al. [8] have investigated the relationship of process parameters on granite surface. Experimental studies have been conducted by using Taguchi's experimental design method. For surface roughness parameter, average roughness (Ra) is used and it is determined that the surface roughness of the specimens increase at higher traverse speed and stand-off distance.

Shanmugam and Masood [1] have investigated the major process parameters of abrasive waterjet machining on the kerf taper angle in cutting of two types of laminated composites: graphite epoxy and glass epoxy. Taguchi experimental design is used to construct the design of experiments for the process parameters. Water pressure, standoff distance and abrasive flow rate are designed by four levels that resulted in 16 combinations. In addition, four levels of traverse speed are added into the experiment that resulted in 64 combinations. Additionally, 14 runs are added to the experimental design for data analysis purpose and totally 78 slots with 20 mm lengths are cut on each composite. Based on the test conditions, a combination of high water pressure, low traverse speed and low standoff distance is recommended to minimise kerf taper angle.

In another study, Shanmugam et al. [9] have used kerf-taper compensation technique in order to reduce the kerf taper on cutting wall. For this purpose there are a total of 16 cuts are performed based on fractional factorial experimental design. As a result, it is found that, kerf taper compensation angle is the most effective parameter on kerf taper angle with an exponent value of 0.94.

Gudimetla et al. [10] have investigated the machinability and kerf formation characteristics of industrial ceramics after cutting with AWJ machine. For this purpose a total of 42 tests are performed using S-Plus software. In the experiments only the effects of water pressure, abrasive flow rate, traverse speed and the jet impingement angle are considered and the others are kept constant. Observations are categorized in kerf geometry, kerf wall and kerf characteristics. Results demonstrate that, the taper angle is proportional to the traverse speed, while it inversely proportional to the water pressure and abrasive flow rate. Also, an increase in traverse speed results in a decrease in surface roughness and higher speeds do not allow the complete machining of the kerf walls. Finally, the total depth of cut increases as the jet impingement angle increased with a peak value and further increase in the jet angle results in a rapid decrease in the depth of cut.

2.3   STUDIES ON MODELLING

Çaydaş and Hasçalık [7] have developed two different models by using ANN and RSM to predict surface roughness in AWJ process. For this purpose, five process parameters, namely, traverse speed, waterjet pressure, stand-off distance, abrasive flow rate and abrasive grid size have designed according to Taguchi's orthogonal array method (L27). 13 of 27 experiments are randomly selected as training data and residuals are used to verify the predicted results. Back propagation architecture with "traingdx" learning rule is chosen in the network. The learning rate and momentum values are selected as 0.9 and 0.2 respectively and after trials minimum error rate is achieved with 22 neurons in the hidden layer. Then, second order RSM model is generated to compare the estimation ability of these models. It is found that the regression model shows a slightly better performance than the ANN model.

Srinivasu and Babu [11] have investigated the effects of wears developed in the nozzle on the depth of cut. For this purpose, three levels of focusing tube diameter, waterjet pressure, traverse speed and abrasive flow rate are design as to full factorial method and a total of $3^4=81$ tests are performed. The results are then used for generating a predictive model in ANN. Back propagation learning rule with sigmoidal transfer function is selected in the architecture of the network. Experimental data is divided as %70 is for training, %10 is for validation and %20 is for testing. Selection of training parameters such as number of hidden layer and number of neurons in each, learning rate, momentum constant and the number of epoch are done according to trial and error method and single hidden layer with 5 neurons shows the best result with the correlation coefficient of 0.967. Finally, the mathematical equation obtained from the network is defined as objective function in genetic algorithm (GA) in order to find the optimum process parameters for desired depth of cut under different diameter of focusing tube.

Davim et al. [12] have generate a predictive model for surface roughness parameters (Ra and Rt) of free machining steel in turning process based on the cutting conditions by using ANN. In order to train the network, three factors (feed rate, cutting speed and depth of cut) with three levels are designed according to Taguchi design of experiment method and a total of 27 tests are performed based on L27 orthogonal array. The network is established using multi layer feed forward architecture with "traingdx" training function. It consists of one input layer with 3 neurons (feed rate, cutting speed and depth of cut), one hidden layer with 16 neurons and one output layer with 2 neurons (Ra and Rt). Learning factors are selected as 0.05 for learning rate, 0.85 for momentum factor and 0.00001 for tolerance of MSE. Based on these parameters, the maximum error percentages are found as 0.75 and 0.58 for Ra and Rt respectively. After that, in addition to data set, three different turning processes are performed in order to compare the results with predicted values. It is found that the results have satisfied the demands with the correlation coefficient of 0.958 and 0.977 for Ra and Rt respectively.

Guzelbey et al. [13] have developed an ANN model in order to estimate the web crippling strength of cold-formed steel decks. It is stated in this study that, selection of appropriate network architecture and training parameters are effective in the performance of the network and they are defined according to try and error method.

6

Also, training of the network may be finished currently before the optimal combination is tried in most of the studies. For this reason, in this study, this gap was tried to fulfil. For this purpose, 228 data was randomly selected for training the network and the rest of 27 data was used for testing. Optimal network wass obtained as quasi-Newton backpropagation (BFGS) with 9-5-1 architecture. In the end of the study, formulation of the prediction model was generated based on the weights and the biases obtained from the Matlab software.

Kok et al. [14] have developed prediction models by using genetic expression programming (GEP) in order to estimate some surface roughness parameters such as Ra, Rz and RSm with respect to experimental results of AWJ machining of 7075 Al alloy composites reinforced with Al_2O_3 particles. In the development of the predictive models, material size, weight fraction of reinforcement particles and depth of cut have taken into account as model variables. Results show that GEP model is successful in estimating surface roughness parameters with a high correlation coefficient that is higher that 90%. Also it is found that surface roughness values increase with an increase in the depth of the cut for all conditions.

CHAPTER 3

ABRASIVE WATERJET MACHINE

3.1 INTRODUCTION

In this chapter, abrasive waterjet cutting machines and their working principles are presented. AWJ cutting machines are considered to consist of water filtration, pressure generation and cutting units. Function of these units and the most important components of each unit are explained. Advantages and disadvantages of these machines are discussed. Application areas of these machines are also mentioned.

3.2 HISTORY OF WATERJETS

Dr. Norman Franz who was a forestry engineer was the first person who studied the use of ultrahigh-pressure (UHP) water as a cutting tool in 1950s. He first tried to cut lumber with ultrahigh pressure. He succeeded to cut wood even some other types of materials. However, components had very low service lives.

In 1970s Dr. Mohammed Hashish created a technique to add abrasives to the waterjets. This and other concepts allowed Yih-Ho Michael Pao to develop commercial ultrahigh-pressure water-jets and abrasive-waterjets into better tools for industrial cutting, drilling, and milling, especially for the flexible factory automation.

Today the water jet is unparalleled in many aspects of cutting and has changed the way many products are manufactured. Many types of water jets exist today, including pure water jets (water only), abrasive water jets, percussive water jets, cavitation jets and hybrid jets among which the first two are the two common jets [15].

3.3 WORKING PRINCIPLES AND COMPONENTS OF AWJ CUTTING SYSTEMS

As shown in Figure 3.1, abrasive waterjet machines consist of three main units. These are water filtration unit, pressure generation unit and cutting unit. Working principles and most important components of each system are explained in the following sections.
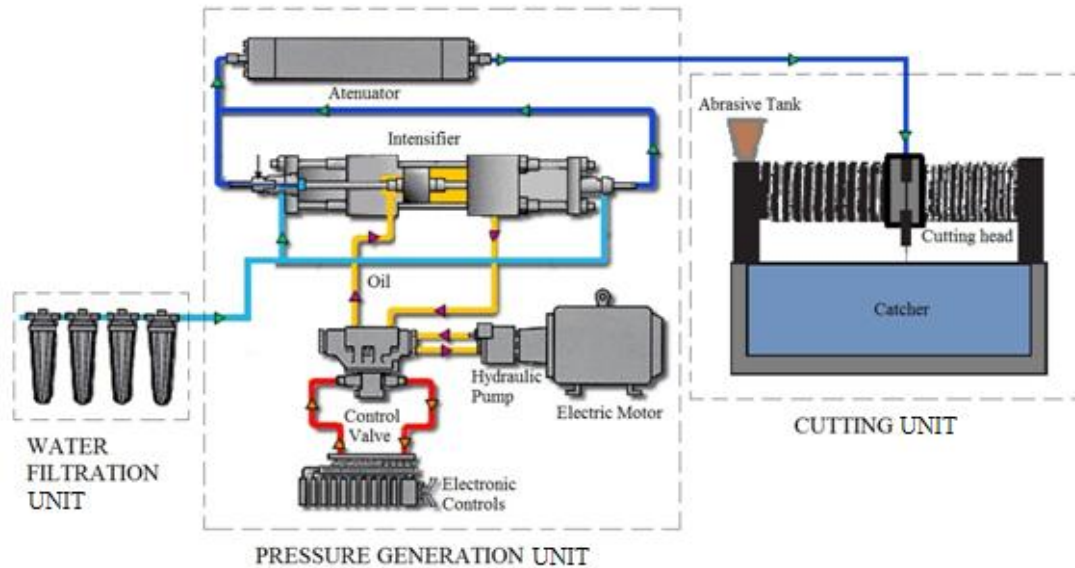
Figure 3.1 Main Systems in AWJ Machine [16]

3.3.1 Water Filtration System

To ensure proper working of the system, the water has to be de-hardened and filtered. It is also important for the nozzle orifice to not to be damaged by foreign materials in the water. Four filters are used for this aim and their sizes are 20μ, 10μ, 5μ and 1μ respectively. So, tap water firstly enters in 20μ filter and finally exits from 1μ filter and it is sent to intensifier.

3.3.2 Pressure Generation System

Pressure generation system consists of electric motor, hydraulic pump, intensifier, accumulator, oil reservoir, manifold, piston biscuit/plunger, valves, electronic controls for valve control, switches and etc. Hydraulic pump powered by the electric

motor pumps the oil to about 200 bar. Then the oil switches the intensifier as one side of the intensifier is the inlet position, the other side is generating ultrahigh pressure water (Referans Fig. 3.3). Then this ultrahigh pressure water is delivered to the attenuator which reduces the pressure fluctuations. During idle times, the water is stored in this tank under pressure to be ready for cutting process [17].

3.3.2.1 Hydraulic Pump

Hydraulic unit consists of an electrically driven, variable displacement and pressure compensated hydraulic pump. Power of the electric motor is about 25 to 200 HP. Typical hydraulic pressures are adjustable to about 200 bar. [17]

3.3.2.2 Intensifier

Intensifier is used to increase the water pressure up to 4000 bar or more. The hydraulic pressure is applied to the low-cylinder of the intensifier, and the water pressure is developed in the high pressure cylinder.
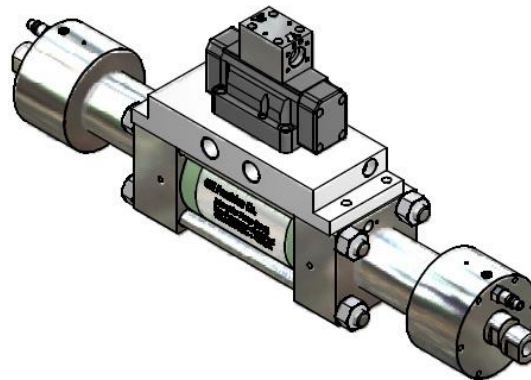
Figure 3.2 Intensifier [18]

Figure 3.3 illustrates the operation of the high- pressure intensifier explained in pressure generating system section. It consists of two terminal small cylinders for water and a large central cylinder for oil.
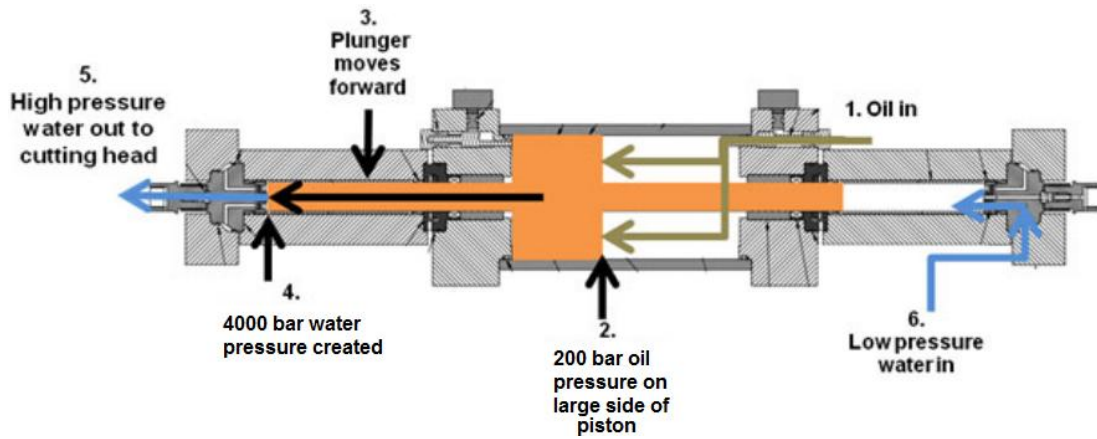
Figure 3.3 HP Intensifier [19]

The pressure increasing is determined by the ratio of the working areas of the two cylinders. The following relationships can be written between pressures and areas [20].

$$p_h.A_p = p_w.A_w \qquad (3.1)$$

$$p_w = p_h.(A_p/A_w) \qquad (3.2)$$

$$p_w = p_h.A_{ratio} \qquad (3.3)$$

Where p_h and p_w are pressures of the hydraulic and the water, A_p and A_w are the cross sectional area of the piston and the cross sectional area of the plunger respectively. If the hydraulic pressure is set to 200 bar and area ratio is 20, water pressure is found as $p_w = 200 \times 20 = 4000$ bar.

3.3.2.3 Attenuator

Attenuator, assembly view is given in Figure 3.4, is used for reducing the pressure fluctuation result from the compression of water. Pressure fluctuations for a particular attenuator (2.49 litre capacity) are illustrated in Figure 3.5. As noticed in this figure, pressure fluctuations are reduced from 150 MPa to 15 MPa which means pressure fluctuations are reduced to 10 percent.
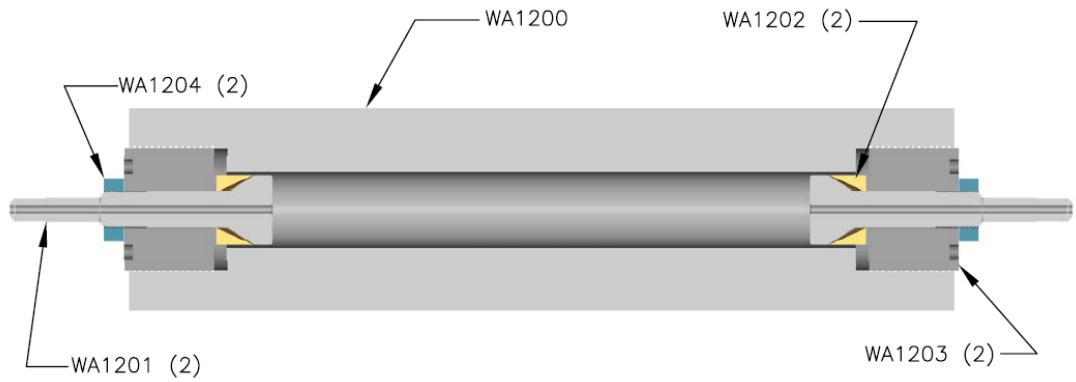
ITEM	WSI NUMBER	COMPONENT DESCRIPTION	QTY
1	WA1200	accumulator body	1
2	WA1201	accumulator port sealing head	2
3	WA1202	accumulator seal ring	2
4	WA1203	accumulator retaining nut	2
5	WA1204	accumulator jam nut	2

Figure 3.4 Assembly View of Attenuator [18]
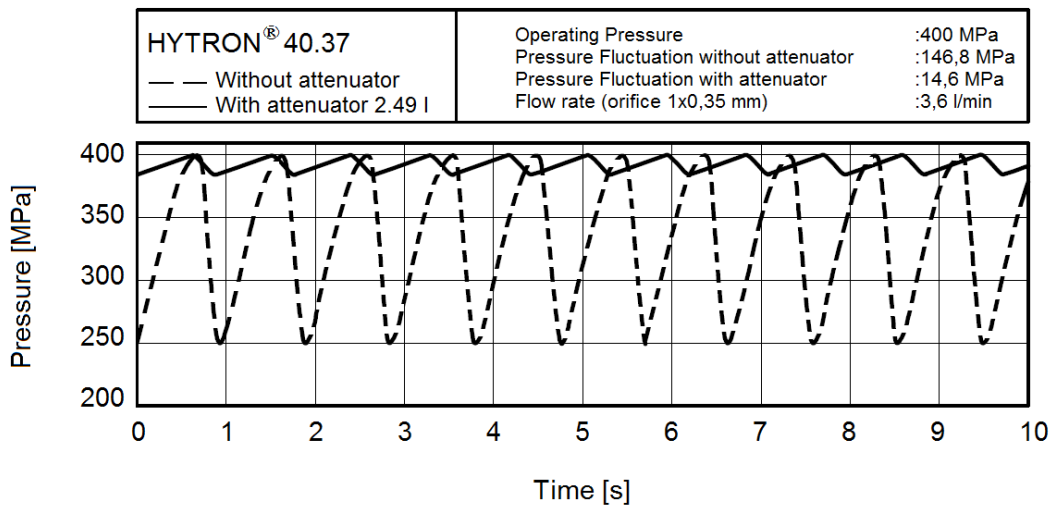
Figure 3.5 Representation of Pressure Fluctuations [19, 21]

3.3.3 Cutting Unit

Travelling of the water runs out at the cutting system. Water sent from the attenuator comes to cutting head. Here, water is mixed with abrasive particles and cutting process is performed by passing them through a narrow hole.

3.3.3.1 Motion and Control Systems

Industrial motion systems of AWJ cutting machine provide the fastest rapid and contouring speeds on the market. The machine provides 2 axes cutting as shown in Figure 3.6. XY tables, sometimes called "flatstock machines," are the most common forms of waterjet motion equipment. These tables are used with pure waterjets to cut gaskets and plastics, rubber and foam. Abrasive waterjets utilize these tables to cut metals, composites, glass stone and ceramics. Flat patterns are cut, in every imaginable design. Abrasive waterjet and pure waterjet tables may be as small as 0.15 x 0.3 meter or as large as a 9 x 30 m. [17]

Figure 3.6 Axes of AWJ Cutting Machine

The basic components of the motion system:

- CNC or PC controller

- Servo motors, usually with closed-loop feedback to ensure position and velocity integrity

- Base unit with linear ways, bearing blocks and ball screw drive

- Bridge unit also with ways, blocks and ball screw

- Catcher tank with material support

The waterjet or the abrasive waterjet must be trapped and dissipated as it exits the material being cut. Catchers are used for this purpose. They also reduce the noise associated with the break-up of the jet after it passes through the target material. Mist or splash back can be a problem if proper catcher is not used.

The catcher tank shown in Figure 3.7 must be deep enough so that the waterjet breaks up before reaching the bottom. This normally requires a depth of 300 to 600 mm, but shorter tanks with steel balls or replaceable hard inserts at the bottom can be used where space is limited.

Figure 3.7 Catcher Tank [22]

3.3.3.2 Cutting Head

The cutting head of AWJ machines include several components:

- The high-pressure delivery component,

- The water orifice or jewel, (generally 1/3 the size of the focusing tube, mixing tube)

- The abrasive feed inlet and nozzle mixing chamber,

- The focusing tube, also referenced as mixing tube and nozzle.
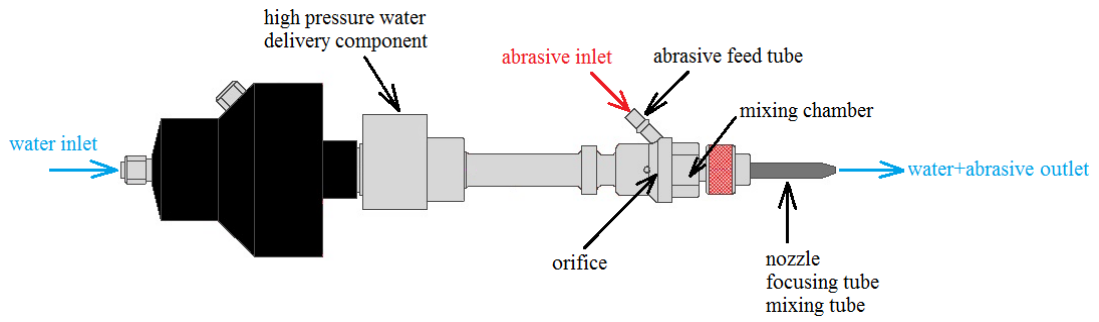
Figure 3.8 AWJ Cutting Head [18]

A high pressure connector is required to connect the nozzle to a supply of high pressure liquid. The high pressure connector is customarily a metal to metal seal. A jewel orifice is used for forming a waterjet. A source of abrasive and means of conveying the abrasive to the nozzle is needed. A means for mixing abrasive and the jet from the jewel orifice and forming a jet are essential functions of the nozzle. The mixing and forming functions are accomplished by an erosion resistant mixing tube. In such a nozzle the liquid pressure is very high. A suitable housing is required to hold all these components together.

High pressurized water sent from attenuator through steel pipe enters cutting head as shown in Figure 3.9. Then it passes through the orifice and comes to mixing chamber. The passage of it through a mixing chamber creates a partial vacuum by venturi effect and entrains abrasive particles from abrasive tank. This particles are mixed and accelerated in the high velocity water stream and they together exit from the mixing tube with the speed of approximately 3 mach [23].
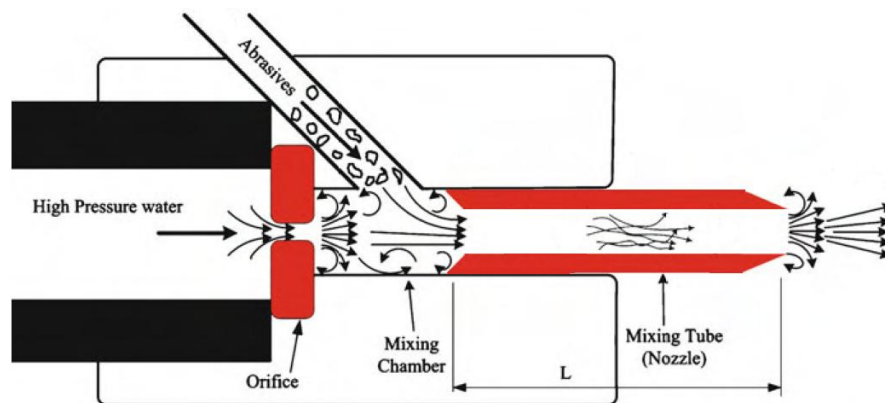
Figure 3.9 Fluid Flow Inside an AWJ Nozzle [23]

15

Orifice materials are usually sapphire, ruby or diamond with sapphire being the most common. Diamond is currently gaining in popularity due to its reliability, extended life, and lower operating cost per hour of usage. Sapphire orifices are prone to chipping and a chipped orifice will also lead to diminished cut quality and shorten the focusing tube life. Some orifice models are given in Figure 3.10.

Figure 3.10 Orifices [24]

AWJ nozzles shown in Figure 3.11 are generally made of steel, composite carbide and special tungsten carbide. Machining pressure determines which material to be used for the nozzle [25].

Figure 3.11 Nozzle (Mixing tube or focusing tube) [25]

Abrasives used in AWJ cutting are generally made of natural sands (garnet, olivin, etc.) or aluminium oxides. Garnet (Ref. Figure 3.12) is the most widely used natural sand in AWJ cutting. It is obtained from riverbeds. After grinding operation, it takes

the form of sharp edged, irregularly shaped. This geometry shows better performance. The largest source of garnet today is garnet rich beach sand which is quite abundant on Indian and Australian coasts and the main producers today are seen to be Australia and India. Also, Rock garnet is used for the longest period of time. This type of garnet is produced in America, China and Western India. [26].

Figure 3.12 Garnet

3.4 COMPARISON OF AWJ CUTTING WITH OTHER METHODS

Waterjet cutting has two equally important benefits to separate it from other machine tools. These are versatility and no heat affected zone [27].

a) Versatility: Waterjets enable you to cut a variety of material with ease using a single machine. Metal, stone, plastic, composite, glass, ceramics, and more can all be cut with waterjet. The same system can also cut a variety of thicknesses that can up to 500 mm with new developed methods.

b) No heat affected zone: Waterjet cutting is a cold cutting process. Heat can have a negative effect changing the structure and properties of metal alloys. Waterjet cutting is high-speed erosion which does not affect the structure and allows for many layers to be cut simultaneously. This is especially useful for cutting tool steel.

The benefits and applications of waterjet technology are limitless and ever-expanding. Listed below are several advantages in addition to versatility and no heat affected zone.

- Unlike machining or grinding, waterjet cutting does not produce any dust or particles which are harmful if inhaled.

17

- Waterjet cutting can be easily automated.

- Any geometry drawn with a drawing programme can be easily transformed CNC codes.

- Extremely detailed geometries can be cut because kerf width in waterjet cutting is very small (0.5 to 1.27 mm).

- Waterjet cutting provides little material loss due to cutting, this increase production efficiency.

- Little or no burr formation after cutting process and it eliminates the other machining operations such as finish sanding and grinding.

- It is easy to mounted waterjet machine with respect to equivalent laser cutting machine. Also it is cheaper.

- No start hole required. It can start directly.

In Table 3.1 and Table 3.2, comparison of waterjet with respect to other methods is given.

Table 3.1 General Comparison of Cutting Systems [28]

	AWJ	Laser	Plasma	Wire Erosion	Milling	Saw	Oxygen
Material thickness	A	C	B	A	B	B	A
Cutting quality	A	A	C	A	B	B	C
Transverse speed	B	A	B	B	B	A	B
Using area	A	D	B	B	B	B	C
Sensitive cutting	A	A	B	A	A	C	D
Extra Process need	A	B	B	B	B	C	C
Burr	B	C	C	A	B	D	B
Flexibility	A	B	C	B	A	C	D
Process time	B	B	D	B	B	A	C
A: Very Good B: Good C: Acceptable D: Unacceptable							

Table 3.2 Comparison of Waterjet With Respect To Plasma, Laser and EDM [27]

	Waterjet	Plasma	Laser	EDM
Process	Erosion process: high speed liquid sandpaper.	Burning/melting process using high temperature ionized gas arc.	Meliting process using concentrated laser light beam.	Erosion process using electrical discharge.
Materials	Any material	Primarily steel, stainless and aluminium.	Primarily steel, stainless and aluminium. Can also cut a variety of other materials	Conductive materials only.
Thickness	Up to 24 inches, virtually any material. Z constraint is only limit to thickness	Up to 2-3 inches, depending on material.	Generally 1 inch or less, depending on materials.	Generally 12 inch or less.
Part Accuracy	Up to .001"	Up to .010"	Up to .001"	Up to .0001"
Machine Setup	Same setup for all materials	Different setup for different jobs	Different gases and parameters for different jobs	Different wire types for different jobs

Waterjet cutting has many advantages with respect to the other cutting methods that are explained above; however, there are also some drawbacks;

- Tapered cutting is a big problem especially cutting of thick materials (Ref. Figure 3.13). There are many studies on reduce or eliminate this problem using some techniques such as oscillation and compensation.
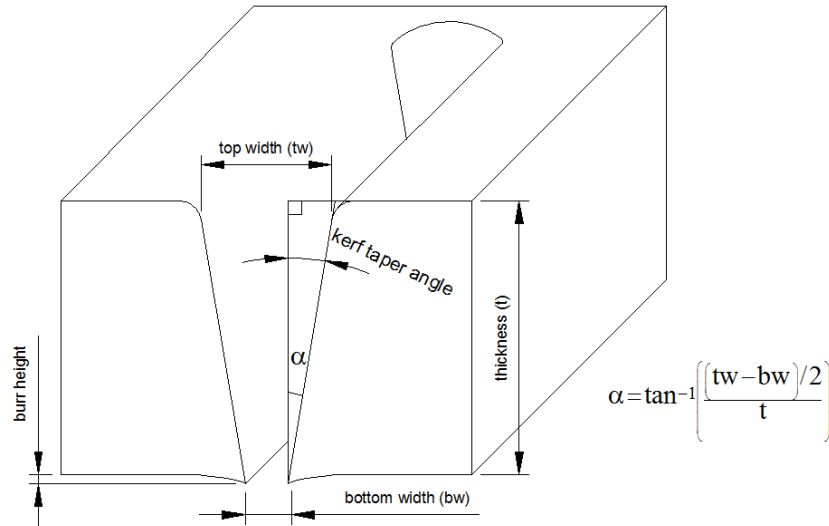
Figure 3.13 Kerf Geometry

- While it is possible to cut tool steels, and other hard materials, the cutting rate has to be greatly reduced, and the time to cut a part can be very long. Because of this, waterjet cutting can be very costly and outweigh the advantages so limited number of materials can be cut economically.

- It creates higher noise than other non-traditional methods.

3.5 APPLICATION OF ABRASIVE WATERJET MACHINING

There are many advantages of abrasive waterjet cutting with respect to the other systems, and these are discussed in the previous section. As a result of these superiorities, this uniqueness technology is preferred for many industries.

Abrasive waterjets extend the applications to harder and denser workpieces. The addition of abrasives allows the cutting of metals, glass and ceramics. Also, some materials such as tool steels, inconel, carbon fiber etc. which are difficult or impossible to be cut with other methods are being cut with abrasive waterjet. The followings can be given for an example of the application field of abrasive waterjet in industrial place.

- Cutting metallic sheet: titanium, aluminium, stainless steel, high tensile strength steel, super alloy: Aircraft industry, rolling stock industry,

20

automobile industry, ship building industry, mechanical engineering industry, steel frame products, bridge manufacturing, ferrous industry, non-ferrous industry, manufacture of metallic products, etc.

- Cutting of glass (wire glas, stained glass, laminated glass): Glass industry, housing industry, interior decoration, advertising, medical appliances manufacture.

- Cutting advanced materials (composite materials, ceramics, etc): Aircraft industry; rolling stock industry, automobile industry, sporting goods industry, fine ceramic industry, ceramic industry, electronic parts industry, optical fiber industry.

- Cutting of building material (board, light weight concrete, etc): Construction industry, housing industry, tile industry [29].

CHAPTER 4

MATERIAL AND METHOD

4.1   INTRODUCTION

This chapter includes the details of equipments, methods and techniques used in the cutting experiments. All the cutting and measuring processes were conducted in the Department of Mechanical Engineering of Gaziantep University. The technical properties of the machine and the material are given in the following tables. In addition to waterjet pressure, stand-off distance and traverse speed, thickness of the material was added as another factor and a total of 81 cutting experiments were performed based on three-level full factorial design method. After surface roughness and kerf geometry measurements, results were tabulated. Main effect and interaction effect plots of process parameters on surface roughness, top width, bottom width and kerf taper angle were drawn by using Minitab software. Based on the figures, effects of process parameters on surface roughness and kerf taper angle were discussed.

4.2   MATERIAL SELECTION

The aluminium alloys (7XXX) have been widely used as structural materials in aerospace and automobile industries due to their excellent properties such as low density, high strength to weight ratio, ductility, toughness, and resistance to fatigue [30]. For this reason, Al 7075-T6 provided from ALTEK METAL (Turkey) was selected as the test specimen material with three different thickness values: 6mm, 8mm and 10 mm. The chemical composition and mechanical properties of the material are given in Table 4.1 and Table 4.2 respectively.

Table 4.1 Chemical Composition of Al 7075 T651 Alloy [31]

Al	Si	Fe	Cu	Mn	Mg	Cr	Zn	Ti
89.57	0.07	0.16	1.60	0.06	2.50	0.20	5.80	0.04

Table 4.2 Mechanical Properties of Al 7075 T651 Alloy [31]

Material	Temper	UTS (Mpa)	Elongation %	0.2% Proof
Al 7075	T651	593	13	521

4.3   AWJ CUTTING MACHINE AND ITS EQUIPMENTS

The cutting experiments were conducted in the Innovation Centre of the Mechanical Engineering Department. As an abrasive waterjet machine, NSJ-2040 (Nevtaş Makine – Figure 4.1), equipped with a dual intensifier with a maximum output pressure of 410 Mpa made in Turkey was used. Specifications of this machine are given in Table 4.3.

Figure 4.1 View of Abrasive Waterjet Machine

Table 4.3 Technical Properties of AWJ Machine [22]

Model	NSJ-2040 (Nevtaş Makine)
Technical Properties	
Machine Dimensions	2000x4000x1650 mm
Cutting Area	1600x3000 mm
Z stroke	180 mm
Axis Speeds	15 m/min
Mini Abrasive Tank	50 kg
Weight (without	4000 kg
Pump Features	
Pump Power	50 HP
Maximum Pressure	4100 bar
Noise Level	<85 db
Weight	750 kg
Oil (used)	Gulf Harmony AW 46
Control & Operating Features	
CNC control unit	ECS
Motion controller	PMAC2 104
Software	NC 400 G-Code
Operating system	MS Windows CE.net

As nozzle and orifice, Kennametal brand Roctec 100 with B-1555426 serial number tungsten carbide nozzle which is 9.45x1.02x76 mm in dimension and Kennametal brand orifice with 0.33 mm diameter were used.

As abrasive particles, garnet sand provided from Supreme Garnet (India) was used. Two mesh size stocks (60 mesh and 80 mesh) are available in the laboratory. After certain number of experimental trials, it was noticed that 80 mesh garnet (grain size is 150-200 μm) gave better surface finish compared to 60 mesh garnet. Hence, 80 mesh garnet was used in all cutting experiments. Physical characteristics and mineralogical composition of the garnet are given in Table 4.4 and Table 4.5 respectively.

Table 4.4 Physical Characteristics of Garnet [32]

Specific Weight	$4.1 \ g/cm^3$
Average Bulk	$2.4 \ g/cm^3$
Hardness	8 (Mohs Scale)

Table 4.5 Mineralogical Composition of Garnet [32]

Garnet (Almandite)	97-98%
Ilmenite	1-2%
Quartz	½%
Others	½%

4.4   SURFACE ROUGHNESS MEASURING

Surface roughness is one of the most important measurements for product quality. There are many parameters to surface roughness. Some of them are briefed below;

- **Roughness average (Ra):** It is the arithmetic average of the absolute values of the roughness profile ordinates.

$$R_a = \frac{1}{1} \int_0^1 |Z(x)| dx$$

(4.1)

- **Root mean square (RMS) roughness (Rq):** It is the root mean square average of the roughness profile.

$$R_q = \sqrt{\frac{1}{1} \int_0^1 Z^2(x) dx}$$

(4.2)

Z(x)= profile ordinates of the roughness profile.
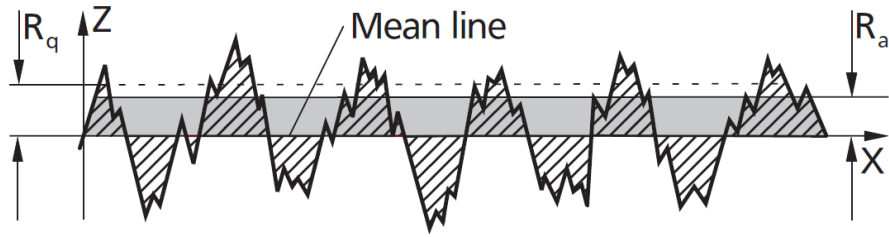
Figure 4.2 Representation of Ra and Rq [33]

- **Single roughness depth (Rzi):** It is the vertical distance between the highest peak and the deepest valley within a sampling length.

- **Mean roughness depth (Rz):** It is the arithmetic mean value of the single roughness depths Rzi of consecutive sampling lengths.

$$R_z = \frac{1}{n}\left(R_{z1} + R_{z2} + \ldots R_{zn}\right)$$

(4.3)

- **Peak Height and peak depth (Rp, Rv):** Rp is the heighest and Rv is the deepest profile peak of the roughness profile within one sampling length. The sum of Rp and Rv is equal the single roughness depth (Rzi).
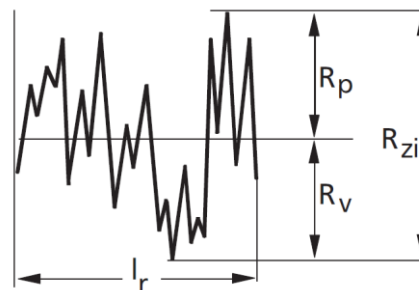
Figure 4.3 Representation of Rp, Rv and Rzi [33]

- **Maximum roughness depth (Rmax):** It is the largest single roughness depth within the evalution length.

- **Maximum height of the profil (Rt):** It is the sum of the highest Rv and deepest Rp along the total length.
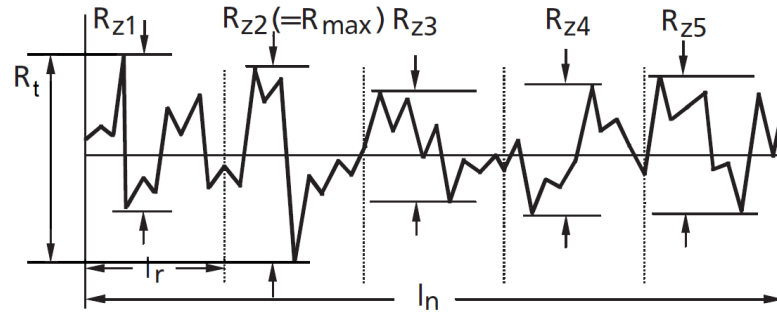
Figure 4.4 Representation of Rz and Rmax [33]

Among these parameters, the most common parameter used in industry is average roughness, R_a. It provides a simple value for accept/reject desicions and available even in the least sophisticated instruments. On the other hand, there are many methods of measuring surface roughness parameters such as stylus type instruments, profile tracing instruments, image processing, etc. In this study stylus type measuring method was applied and for this aim Mahr stylus instrument (MarSurf XR 20 with GD 25) which is available in our mechanical laboratory was used (Ref Figure 4.5). Some properties of the instrument and parameters used in the measurements are given in Table 4.6.
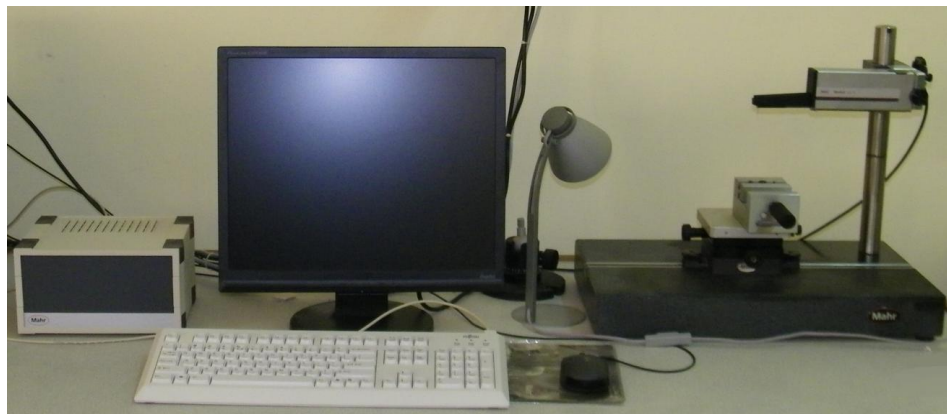
Figure 4.5 Mahr Stylus Instrument

Table 4.6 Measuring Parameters

Software	MarTalk$^{®}$
Drive Unit	GD 25
Prob	MFW-250:1(#6851855)-1.0%
Traversing Speed [V_t] (mm/sec)	0.5
Traversing Length [L_t] (mm)	17.5
Cut off length [λ_c] (mm)	2.5x5

4.4.1   Determination of Region for Surface Roughness Measurements

In AWJ cutting, three distinct cutting zones are identified as demonstrated in Figure 4.6. They are: (1) an initial damage region (IDR), which is cutting zone at shallow angles of attack; (2) a smooth cutting region (SCR), which is cutting zone at large angles of attack; (3) a rough cutting region (RCR), which is the jet upward deflection zone where the waviness is concentrated; and it is found that surface roughness values of each region shows variation [34]. Also, Külekci and Akkurt [5] had suggested that surface profile is harmonic in the initial damage region (IDR).
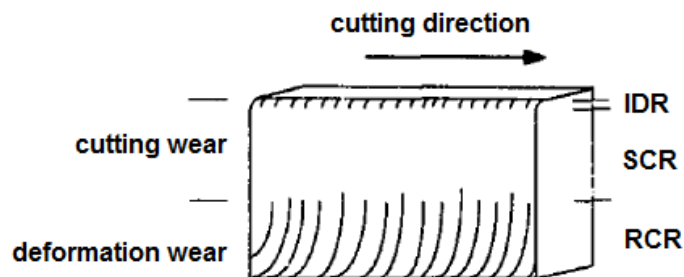
Figure 4.6 Cutting Regions

In the evaluation of the effects of process parameters on the surface roughness, we have to decide from which region that the measurements will be taken. This requires the determination of the above mentioned regions. For that we consider two extreme cutting conditions for three specimens with different thicknesses (6, 8 and 10 mm). One extreme (called "low effective" condition) is where pressure is minimum, traverse speed and stand-off distance are maximum. The other extreme (called "high effective" condition) is where pressure is maximum, traverse speed and stand-off distance are minimum. These conditions are summarized in Table 4.7 Surface

28

roughness measurements with 1 mm interval starting from top are illustrated in Table 4.8.

Table 4.7 Machining Settings and Corresponding Effective Conditions for Selected Parts

Exp	t (mm)	P (bar)	V (mm/min)	h (mm)	Effect
1	6	2000	140	7	Low
2	8	2000	140	7	Low
3	10	2000	140	7	Low
4	6	3400	30	3	High
5	8	3400	30	3	High
6	10	3400	30	3	High

Table 4.8 Surface Roughness Results of Selected Parts (from top to bottom with 1 mm interval)

	Exp	1 mm	2 mm	3 mm	4 mm	5 mm	6 mm	7 mm	8 mm	9 mm
Low E.	1	5,579	5,663	7,450	8,952	8,652				
	2	5,391	5,676	7,312	8,168	8,899	11,055	13,784		
	3	5,250	5,727	6,163	6,473	8,166	8,3811	10,414	14,613	19,749
High E.	4	3,152	3,047	3,780	4,492	4,088				
	5	3,145	3,399	3,635	3,766	4,070	3,780	3,884		
	6	3,114	3,221	3,735	3,583	4,089	3,906	3,897	3,928	3,8299

Surface roughness values in Table 4.8 are plotted and illustrated in Figure 4.7 and Figure 4.8 for "low" effective and "high" effective conditions respectively. Initial damage region (IDR) is not revealed in this measurement range that may be found in the depth of smaller than 1 mm. Also it is found that the smooth cutting region (SCR) takes the place of smooth cutting region above the depth of 2 mm for both conditions. For this reason, the depth of 2 mm is found appropriate as the measurement depth for each cutting experiments. Also, cut-off distance is selected as 2.5 mm according to ISO 4288 (Ref. Table 4.9).

From Table 4.8 it can be seen that under low effective condition, ratio of SCR/RCR are 2/4, 2/6, 2/8 respectively. Similar trend can be observed in high effective

condition. That is, as the thickness increases the region of rough cutting is being extended.
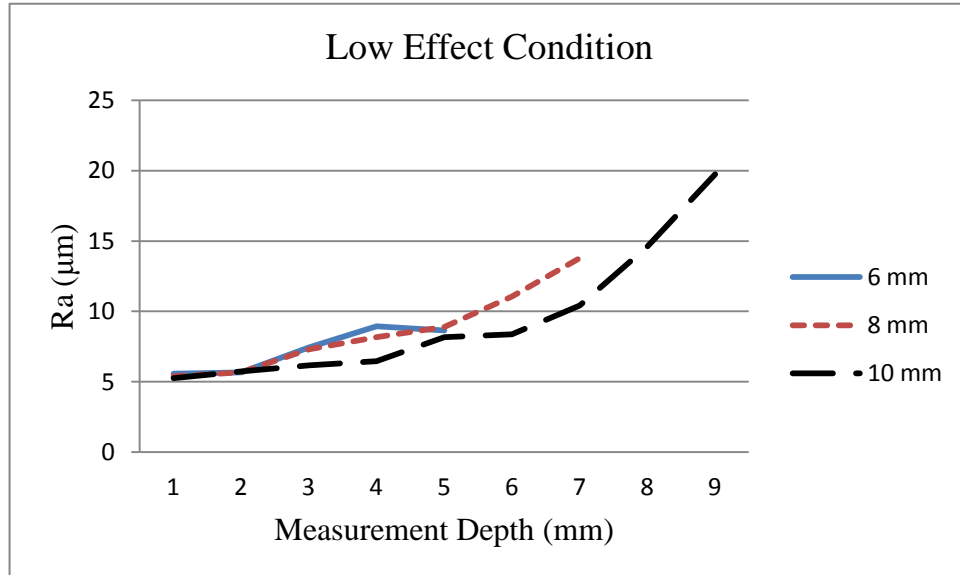
Figure 4.7 Surface Roughness Variations for "Low" Effective Condition
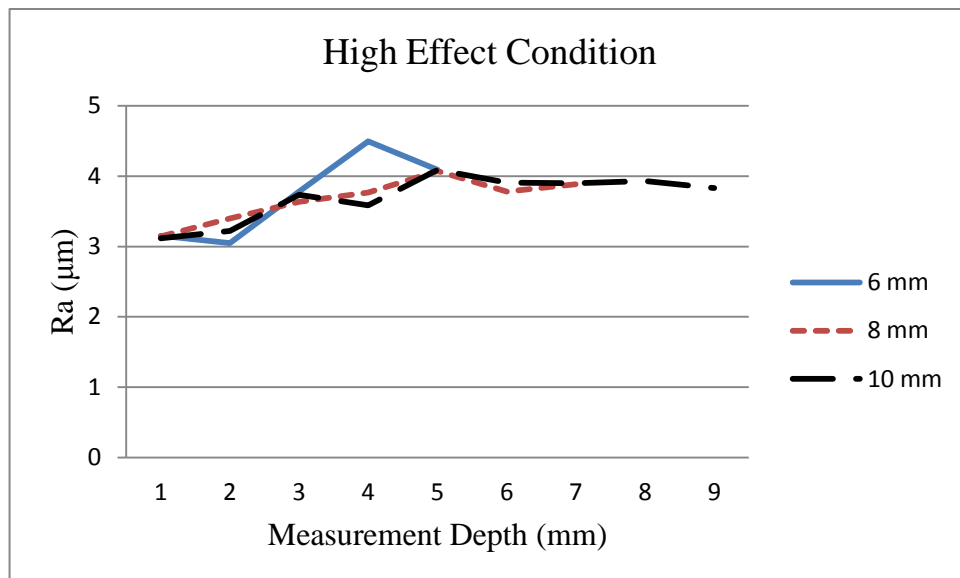
Figure 4.8 Surface Roughness Variations for "High" Effective Condition

Table 4.9 Selection of Cut-Off Distance [33]

Periodic	Nonperiodic profiles		Cut-off	Evaluation length
R_{sm} (mm)	R_z (µm)	R_a (µm)	λ_c (mm)	l_n (mm)
over .013 up to 0.04	up to 0.1	up to 0.02	0.08	0.4
over 0.04 up to 0.13	over 0.1 up to 0.5	over 0.02 up to 0.1	0.25	1.25
over 0.13 up to 0.4	over 0.5 up to 10	over 0.1 up to 2	0.8	4
over 0.4 up to 1.3	over 10 up to 50	over 2 up to 10	2.5	12.5
over 1.3 up to 4	over 50 up to 200	over 10 up to 80	8	40

4.5   KERF GEOMETRY MEASURING

Kerf profile produced in AWJ cutting is wider at the top, and gets narrow towards the bottom as shown in Figure 4.9 (a). This is because; the jet loses its kinetic energy from top to bottom. Also, the particle velocity at any cross-section of a jet should vary from zero at the nozzle wall to a maximum at the jet centre [35]. This velocity distribution corresponds to an energy or strength distribution in the jet. The inner contoured regions of the jet, as shown in Figure 4.9 (b) noted as ''effective width'', have higher velocities than the outer regions, are resulted in tapered cuts on the material [1]. In addition to them, only effective width causes kerf creation [36, 1].

(a) Kerf Profile

(b) Relative strength zones in a waterjet
[Hashish and Plessis, 1979]
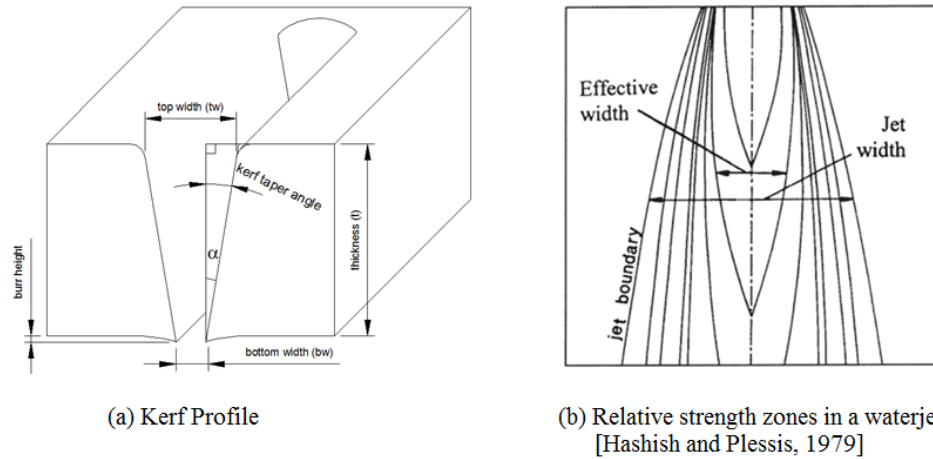
Figure 4.9 Kerf Formation in Waterjet Cutting

In order to measure and investigate kerf geometry, hp scanjet 5500c scanner was used. Scanning process was performed in 600 dpi resolution and images were saved as "jpg" format. The images opened with Autocad 2012® software with a scale factor of 1. Measurements were taken at top and bottom points of the slot as illustrated in Figure 4.10 and results are recorded. Based on these data, kerf taper angle values were then calculated by using the following formula.

$$\theta = \tan^{-1}\left(\frac{(tw - bw)/2}{t}\right) \qquad (4.4)$$
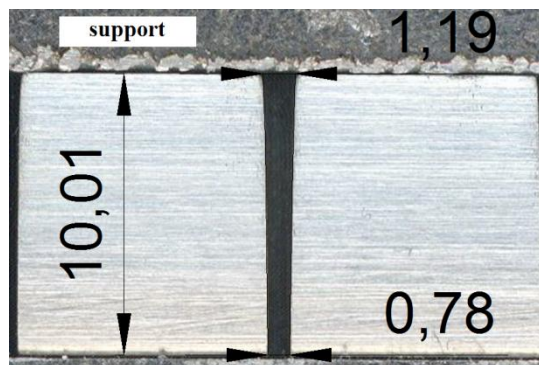
Figure 4.10 Measurement of Kerf Geometry (Experimental no: 77)

4.6 DESIGN OF EXPERIMENT

AWJ cutting involves a large number of variables as mentioned in the first chapter and virtually all these variables affect the cutting quality and kerf formation. Water pressure, traverse speed and stand-off distance are the three factors considered in

most of the studies. In this study, thickness of the material is added as another factor to the process parameters and the other parameters including orifice diameter (0.33 mm), mixing tube (nozzle) diameter (1.02 mm), length of mixing tube (76 mm), abrasive grit size (80 mesh), abrasive flow rate (0.3 kg/min) and abrasive type (garnet) were considered as the constant parameters.

Levels of selected process parameters were identified by going through a series of experiments. Firstly, the levels of water pressure were determined according to pressure capacity of the hydraulic unit and thickness of the material. For safety reasons, 3400 bar was taken as an upper limit for the pressure. On the other hand, it was seen that, pressure under 2000 bar was not adequate for cutting the material thoroughly. Consequently, pressure values were determined as 2000, 2700 and 3400 bar. In order to determine the stand-off distance values, firstly the lower limit was defined as 3 mm due to heating of the nozzle. Then, 7 mm was selected for the upper level because it was realized that 2000 bar pressure was not able to cut the material above this value. As a result, they were selected as 3 mm 5 mm and 7 mm. For the determination of the traverse speed levels, the worst conditions, namely, when the pressure is 2000 bar, thickness of the material is 10 mm and the stand-off distance is 7 mm are considered. From this combination, maximum traverse speed range was found as 150-160 mm/min. However, because of the uncertainties that may lead to uncut specimens, upper limit of the traverse speed was selected as 140 mm/min and the other levels were adjusted as 85 mm/min and 30 mm/min. All these four parameters and their factor levels are summarized in Table 4.10.

Table 4.10 Machining Settings Used in the Experiments

Symbol	Parameters	Level 1	Level 2	Level 3
t	Material thickness (mm)	6	8	10
P	Waterjet pressure (bar)	2000	2700	3400
h	Standoff distance (mm)	3	5	7
V	Traverse speed (mm/min)	30	85	140

Although there are some fractionated factorial designs techniques which reduce the number of experiment in order to save on experimental cost and process time, any of these methods was preferred in this study. There are two reasons of it: First is to investigate the effects of the parameters in more detail and second is to provide

adequate data for ANN explained in the next chapter. Therefore, full factorial experimental design was used and totally 3^4 (81) experiments were conducted. The layout of the experimental design set is listed in Table 4.11.

Table 4.11 Experimental Design

Exp	t	P	h	V	Exp	t	P	h	V	Exp	t	P	h	V
1	6	2000	3	30	28	8	2000	3	30	55	10	2000	3	30
2	6	2000	3	85	29	8	2000	3	85	56	10	2000	3	85
3	6	2000	3	140	30	8	2000	3	140	57	10	2000	3	140
4	6	2000	5	30	31	8	2000	5	30	58	10	2000	5	30
5	6	2000	5	85	32	8	2000	5	85	59	10	2000	5	85
6	6	2000	5	140	33	8	2000	5	140	60	10	2000	5	140
7	6	2000	7	30	34	8	2000	7	30	61	10	2000	7	30
8	6	2000	7	85	35	8	2000	7	85	62	10	2000	7	85
9	6	2000	7	140	36	8	2000	7	140	63	10	2000	7	140
10	6	2700	3	30	37	8	2700	3	30	64	10	2700	3	30
11	6	2700	3	85	38	8	2700	3	85	65	10	2700	3	85
12	6	2700	3	140	39	8	2700	3	140	66	10	2700	3	140
13	6	2700	5	30	40	8	2700	5	30	67	10	2700	5	30
14	6	2700	5	85	41	8	2700	5	85	68	10	2700	5	85
15	6	2700	5	140	42	8	2700	5	140	69	10	2700	5	140
16	6	2700	7	30	43	8	2700	7	30	70	10	2700	7	30
17	6	2700	7	85	44	8	2700	7	85	71	10	2700	7	85
18	6	2700	7	140	45	8	2700	7	140	72	10	2700	7	140
19	6	3400	3	30	46	8	3400	3	30	73	10	3400	3	30
20	6	3400	3	85	47	8	3400	3	85	74	10	3400	3	85
21	6	3400	3	140	48	8	3400	3	140	75	10	3400	3	140
22	6	3400	5	30	49	8	3400	5	30	76	10	3400	5	30
23	6	3400	5	85	50	8	3400	5	85	77	10	3400	5	85
24	6	3400	5	140	51	8	3400	5	140	78	10	3400	5	140
25	6	3400	7	30	52	8	3400	7	30	79	10	3400	7	30
26	6	3400	7	85	53	8	3400	7	85	80	10	3400	7	85
27	6	3400	7	140	54	8	3400	7	140	81	10	3400	7	140

4.7 EXPERIMENTAL PROCEDURE

In this section experimental procedure is explained in detail. The procedure starts with the preparation of experimental set-up and ends with finishing of cutting operation.

- Grates of the machine were adjusted as prevent the differences in "z direction" when the workpiece is mounted. For this aim, additional parts were welded on the grates using bubble level. Also required area on the grates for cutting operation was determined as 250x600 mm and the materials were cut at these dimensions.

- The AWJ machine was prepared to cutting operation. For this purpose, filters and hoses were replaced with new ones, nozzle and orifice were mounted and oil and abrasive sands (garnet) were added.

- The cutting experiments were performed as shown in the Figure 4.11. It was considered that cutting of 30 mm length for surface roughness measurements and 10 mm length for kerf geometry measurements were adequate.
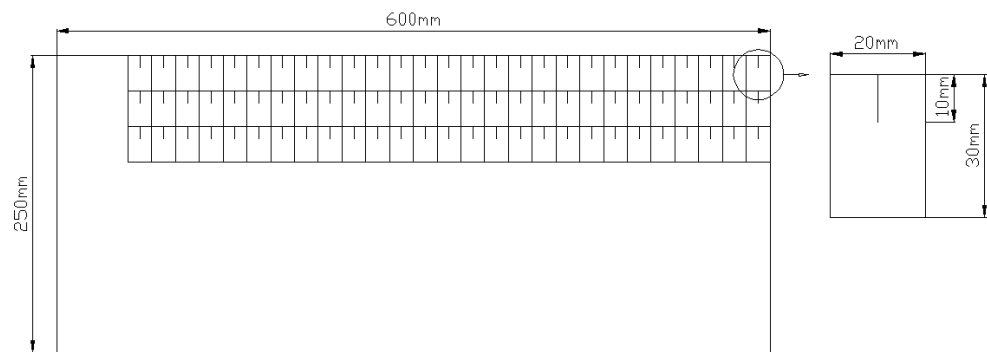
Figure 4.11 Cutting Schema

Figure 4.12 Test Pieces

- While cutting operations, cutting parameters were changed in a particular order. Traverse speed was the first and stand-off distance and waterjet

pressure follows as given in Table 4.12. 10 mm initial space in +Y direction is given in the cutting experiments.

Table 4.12 CNC Codes of First 9 Cutting Process

		V (mm/min)										
		N1F30				N6F85				N11F140		
h (mm)	3	N2	G0	X590	Y260	N7	G0	X570	Y260	N12	G0	X550	Y260
		N3	G1	X590	Y240	N8	G1	X570	Y240	N13	G1	X550	Y240
		N4	G0	X580	Y260	N9	G0	X560	Y260	N14	G0	X540	Y260
		N5	G1	X580	Y220	N10	G1	X560	Y220	N15	G1	X540	Y220
		N16F30				N21F85				N26F140		
	5	N17	G0	X530	Y260	N22	G0	X510	Y260	N27	G0	X490	Y260
		N18	G1	X530	Y240	N23	G1	X510	Y240	N28	G1	X490	Y240
		N19	G0	X520	Y260	N24	G0	X500	Y260	N29	G0	X480	Y260
		N20	G1	X520	Y220	N25	G1	X500	Y220	N30	G1	X480	Y220
		N31F30				N36F85				N41F140		
	7	N32	G0	X470	Y260	N37	G0	X450	Y260	N42	G0	X430	Y260
		N33	G1	X470	Y240	N38	G1	X450	Y240	N43	G1	X430	Y240
		N34	G0	X460	Y260	N39	G0	X440	Y260	N44	G0	X420	Y260
		N35	G1	X460	Y220	N40	G1	X440	Y220	N45	G1	X420	Y220
		P=2000 bar										

- After each cutting of 27 specimens, material block were grinded to measure the kerf geometry accurately.

- During cutting process, special attention was paid to wait same period of time while chancing pressure from low to high value.

4.8   EXPERIMENTAL RESULTS AND DISCUSSIONS

Experimental results of average roughness (Ra) and kerf taper angle (θ) for different process parameters (t, P, h, V) are given in Table 4.13 and Table 4.14 respectively. The relationship between these parameters has been investigated by using Minitab® software. Main effect and interaction effect plots are drawn to compare the relative strength of the effects across the factors.

4.8.1 Experimental Results for Roughness Average (Ra)

Table 4.13 Experimental Results of Ra

Exp	t (mm)	P (bar)	h (mm)	V (mm)	Ra (μm)	Exp	t (mm)	P (bar)	h (mm)	V (mm)	Ra (μm)
1	6	2000	3	30	3,239	42	8	2700	5	140	5,166
2	6	2000	3	85	4,296	43	8	2700	7	30	4,061
3	6	2000	3	140	4,417	44	8	2700	7	85	5,189
4	6	2000	5	30	4,383	45	8	2700	7	140	5,345
5	6	2000	5	85	5,181	46	8	3400	3	30	3,399
6	6	2000	5	140	5,490	47	8	3400	3	85	3,643
7	6	2000	7	30	5,025	48	8	3400	3	140	4,138
8	6	2000	7	85	5,204	49	8	3400	5	30	3,897
9	6	2000	7	140	5,663	50	8	3400	5	85	4,339
10	6	2700	3	30	3,527	51	8	3400	5	140	4,580
11	6	2700	3	85	4,054	52	8	3400	7	30	4,106
12	6	2700	3	140	4,153	53	8	3400	7	85	4,796
13	6	2700	5	30	3,818	54	8	3400	7	140	5,729
14	6	2700	5	85	4,834	55	10	2000	3	30	3,332
15	6	2700	5	140	5,823	56	10	2000	3	85	4,180
16	6	2700	7	30	4,089	57	10	2000	3	140	5,156
17	6	2700	7	85	5,269	58	10	2000	5	30	3,906
18	6	2700	7	140	5,434	59	10	2000	5	85	4,456
19	6	3400	3	30	3,047	60	10	2000	5	140	4,891
20	6	3400	3	85	3,349	61	10	2000	7	30	4,439
21	6	3400	3	140	3,536	62	10	2000	7	85	5,500
22	6	3400	5	30	3,654	63	10	2000	7	140	5,727
23	6	3400	5	85	3,724	64	10	2700	3	30	3,583
24	6	3400	5	140	4,114	65	10	2700	3	85	4,129
25	6	3400	7	30	4,327	66	10	2700	3	140	4,507
26	6	3400	7	85	4,528	67	10	2700	5	30	4,346
27	6	3400	7	140	4,998	68	10	2700	5	85	4,669
28	8	2000	3	30	3,793	69	10	2700	5	140	5,429
29	8	2000	3	85	4,489	70	10	2700	7	30	4,794
30	8	2000	3	140	5,536	71	10	2700	7	85	5,488
31	8	2000	5	30	4,213	72	10	2700	7	140	5,785
32	8	2000	5	85	5,111	73	10	3400	3	30	3,221
33	8	2000	5	140	5,432	74	10	3400	3	85	4,078
34	8	2000	7	30	4,419	75	10	3400	3	140	4,434
35	8	2000	7	85	5,276	76	10	3400	5	30	3,555
36	8	2000	7	140	5,676	77	10	3400	5	85	4,316
37	8	2700	3	30	3,558	78	10	3400	5	140	4,486
38	8	2700	3	85	4,078	79	10	3400	7	30	3,780
39	8	2700	3	140	4,444	80	10	3400	7	85	4,930
40	8	2700	5	30	3,845	81	10	3400	7	140	4,953
41	8	2700	5	85	4,158						

In Figure 4.13, main effects of process parameters into mean roughness values are given. It is clear from the figure that, traverse speed, stand-off distance and water pressure are effective parameters on surface roughness. Increase in the traverse speed and stand-off distance result in an increase in the surface roughness. On the other hand, an increase in the water pressure results in a decrease in the surface roughness while the thickness of the material does not change Ra value significantly. However, increase in thickness from 6 to 8 mm result in a little increase in Ra while with a further increase in the thickness, there is almost no variation.
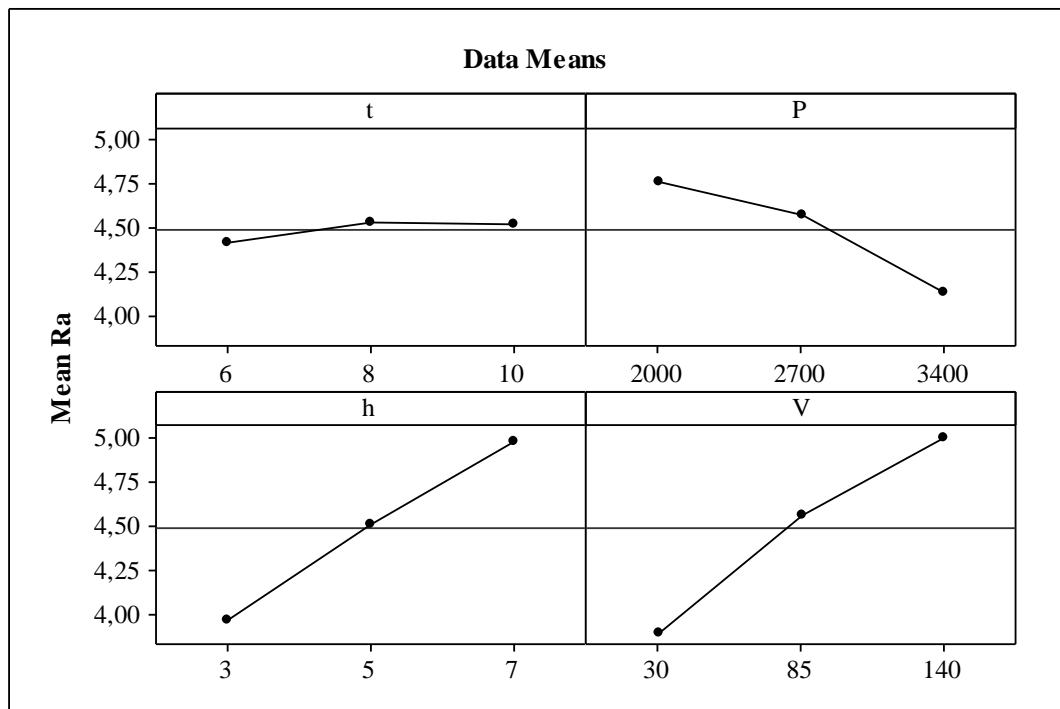
Figure 4.13 Main Effects of Process Parameters on Ra

In interaction plots, the input variables are considered together and their effects can be investigated in more details. While drawing these plots two variables and their corresponding average surface roughness values are taken. Figure 4.14 shows the overall interactions between process parameters. It is shown in the figure that, surface roughness has the tendency to increase with an increase of traverse speed. This may be due to the fact that process time decreases with an increase in the traverse speed and as a result of it the jet leaves the cutting zone before the cutting operation completely finishes. Thus, the particles which do not undergo the erosion of the jet cause rougher surface. Stand-off distance is also found to be effective on the surface roughness for all condition. This can be explained with strength zone

phenomena mentioned in Section 4.5 (kerf geometry measuring). Increase in the stand-off distance causes larger but less effective jet width and this leads not only wider kerf, but also rougher surface. The third important factor is waterjet pressure in this group. Surface roughness decreases with an increase in the water pressure. This is because, with an increase in the pressure, effective jet width enlarges. As a result, particle erosion increases similar to the effect of the traverse speed. However the situation is a bit different when the thickness of the material is 10 mm. In this case, surface roughness initially increases when the pressure increases from 2000 bar to 2700 bar, with a further increase in the pressure, the surface roughness decreases.
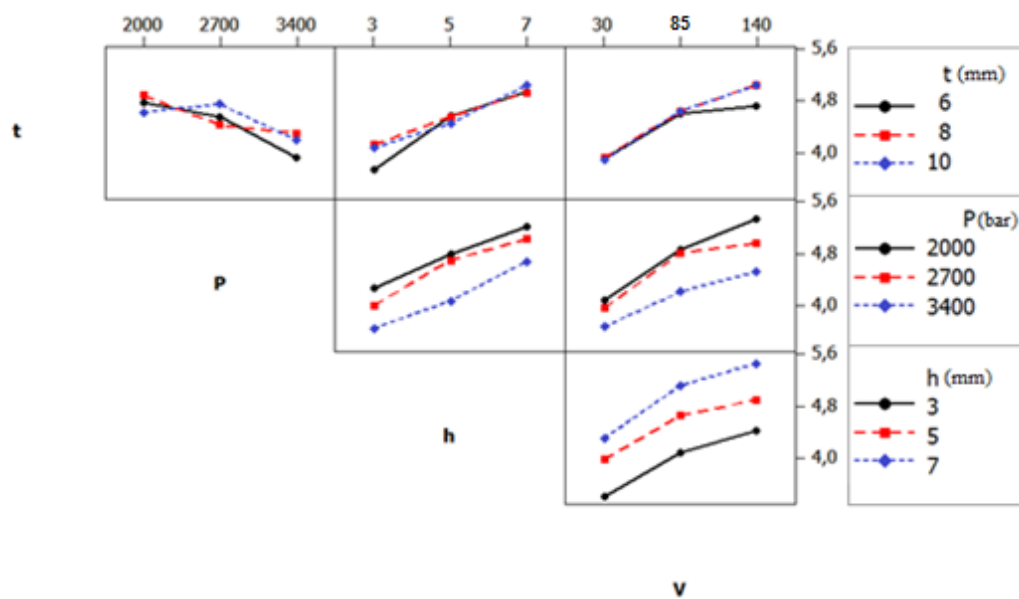
Figure 4.14 Interaction Plots of the Parameters

A little alteration was observed on the surface roughness of the specimens with different thicknesses. Although minimum surface roughness values were recorded when the thickness is 6 mm, the effect of the thickness may be omitted.

4.8.2 Experimental Results for Kerf Geometry (Top Width (tw), Bottom Width (bw) and Kerf Taper Angle (θ))

Table 4.14 Experimental Results of Kerf Geometry

Exp	t (mm)	P (bar)	h (mm)	V (mm)	tw (mm)	bw (mm)	θ (^{0})
1	6	2000	3	30	1,08	0,84	1,15
2	6	2000	3	85	1,05	0,71	1,62
3	6	2000	3	140	1,02	0,65	1,77
4	6	2000	5	30	1,26	0,92	1,62
5	6	2000	5	85	1,15	0,74	1,96
6	6	2000	5	140	1,10	0,62	2,29
7	6	2000	7	30	1,38	1,01	1,77
8	6	2000	7	85	1,24	0,76	2,29
9	6	2000	7	140	1,11	0,61	2,39
10	6	2700	3	30	1,14	0,94	0,95
11	6	2700	3	85	1,12	0,80	1,53
12	6	2700	3	140	1,08	0,72	1,72
13	6	2700	5	30	1,29	1,03	1,24
14	6	2700	5	85	1,22	0,83	1,86
15	6	2700	5	140	1,14	0,72	2,00
16	6	2700	7	30	1,42	1,10	1,53
17	6	2700	7	85	1,31	0,86	2,15
18	6	2700	7	140	1,24	0,82	2,00
19	6	3400	3	30	1,14	0,88	1,24
20	6	3400	3	85	1,09	0,84	1,19
21	6	3400	3	140	1,09	0,77	1,53
22	6	3400	5	30	1,30	1,10	0,95
23	6	3400	5	85	1,22	0,93	1,38
24	6	3400	5	140	1,16	0,81	1,67
25	6	3400	7	30	1,47	1,16	1,48
26	6	3400	7	85	1,31	0,91	1,91
27	6	3400	7	140	1,25	0,83	2,00
28	8	2000	3	30	1,12	0,86	0,93
29	8	2000	3	85	1,08	0,66	1,50
30	8	2000	3	140	1,05	0,48	2,04
31	8	2000	5	30	1,26	0,91	1,25
32	8	2000	5	85	1,16	0,70	1,65
33	8	2000	5	140	1,09	0,53	2,00
34	8	2000	7	30	1,41	0,95	1,65
35	8	2000	7	85	1,28	0,73	1,97
36	8	2000	7	140	1,24	0,56	2,43
37	8	2700	3	30	1,15	0,89	0,93
38	8	2700	3	85	1,08	0,72	1,29
39	8	2700	3	140	1,05	0,68	1,32
40	8	2700	5	30	1,30	0,98	1,15
41	8	2700	5	85	1,14	0,80	1,22

Exp	t (mm)	P (bar)	h (mm)	V (mm)	tw (mm)	bw (mm)	θ (⁰)
42	8	2700	5	140	1,13	0,66	1,68
43	8	2700	7	30	1,43	1,09	1,22
44	8	2700	7	85	1,30	0,82	1,72
45	8	2700	7	140	1,08	0,62	1,65
46	8	3400	3	30	1,13	0,94	0,68
47	8	3400	3	85	1,06	0,71	1,25
48	8	3400	3	140	1,05	0,65	1,43
49	8	3400	5	30	1,24	0,97	0,97
50	8	3400	5	85	1,14	0,79	1,25
51	8	3400	5	140	1,09	0,68	1,47
52	8	3400	7	30	1,36	0,99	1,32
53	8	3400	7	85	1,22	0,78	1,58
54	8	3400	7	140	1,18	0,67	1,83
55	10	2000	3	30	1,12	0,79	0,95
56	10	2000	3	85	1,08	0,57	1,46
57	10	2000	3	140	1,00	0,39	1,75
58	10	2000	5	30	1,25	0,88	1,06
59	10	2000	5	85	1,18	0,63	1,58
60	10	2000	5	140	1,15	0,40	2,15
61	10	2000	7	30	1,36	0,90	1,32
62	10	2000	7	85	1,25	0,64	1,75
63	10	2000	7	140	1,18	0,41	2,20
64	10	2700	3	30	1,13	0,89	0,69
65	10	2700	3	85	1,06	0,71	1,00
66	10	2700	3	140	1,03	0,53	1,43
67	10	2700	5	30	1,30	0,95	1,00
68	10	2700	5	85	1,18	0,73	1,29
69	10	2700	5	140	1,18	0,55	1,80
70	10	2700	7	30	1,44	1,02	1,20
71	10	2700	7	85	1,12	0,75	1,06
72	10	2700	7	140	1,15	0,55	1,72
73	10	3400	3	30	1,15	0,90	0,72
74	10	3400	3	85	1,09	0,74	1,00
75	10	3400	3	140	1,04	0,49	1,58
76	10	3400	5	30	1,31	1,01	0,86
77	10	3400	5	85	1,19	0,78	1,17
78	10	3400	5	140	1,14	0,63	1,46
79	10	3400	7	30	1,50	1,08	1,20
80	10	3400	7	85	1,36	0,86	1,43
81	10	3400	7	140	1,28	0,71	1,63

Measurement results of kerf geometry are listed in Table 4.14. In this table, the corresponding terms of tw, bw and θ are top width, bottom width and kerf taper angle respectively. Also main effect plots of top width, bottom width and kerf taper angle are given in Figure 4.15 to 4.17.
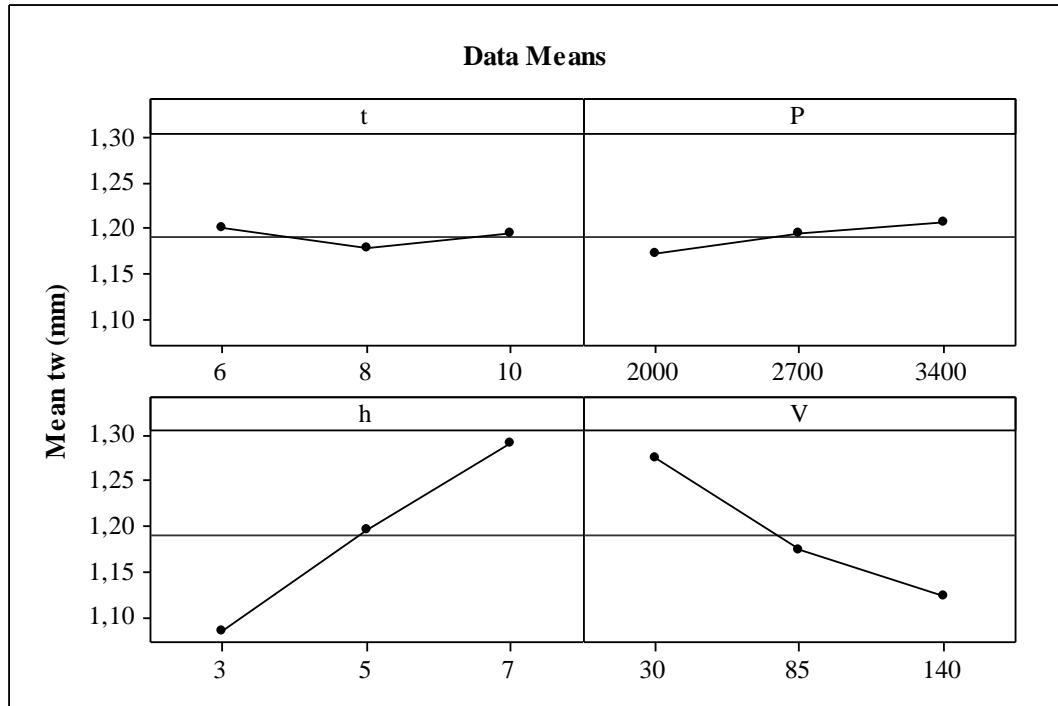
Figure 4.15 Main Effects of Process Parameters on Top Width (tw)

It is seen from the Figure 4.15 that, stand-off distance, traverse speed and waterjet pressure are three effective factors on top width formation while thickness of the material is not influential. Also stand-off distance is found as the most effective parameter. Increase in each of stand-off or waterjet pressure results in an increase in top width. In contrast, top with is narrowing with an increase in the traverse speed.

In Figure 4.16, main effects of process parameters on mean bottom width values are illustrated. Results are not very different compared to the results of top width. Only the significant difference is seen in the effect of material thickness. Bottom width is narrowing with an increase in the material thickness. This may explained with kinetic energy theorem. Overall energy of the jet decreases in the each level of the thickness while it is spent on eroding the material. So, reduced kinetic energy causes narrower width. Also, further increasing in the material thickness leads to uncut specimens.
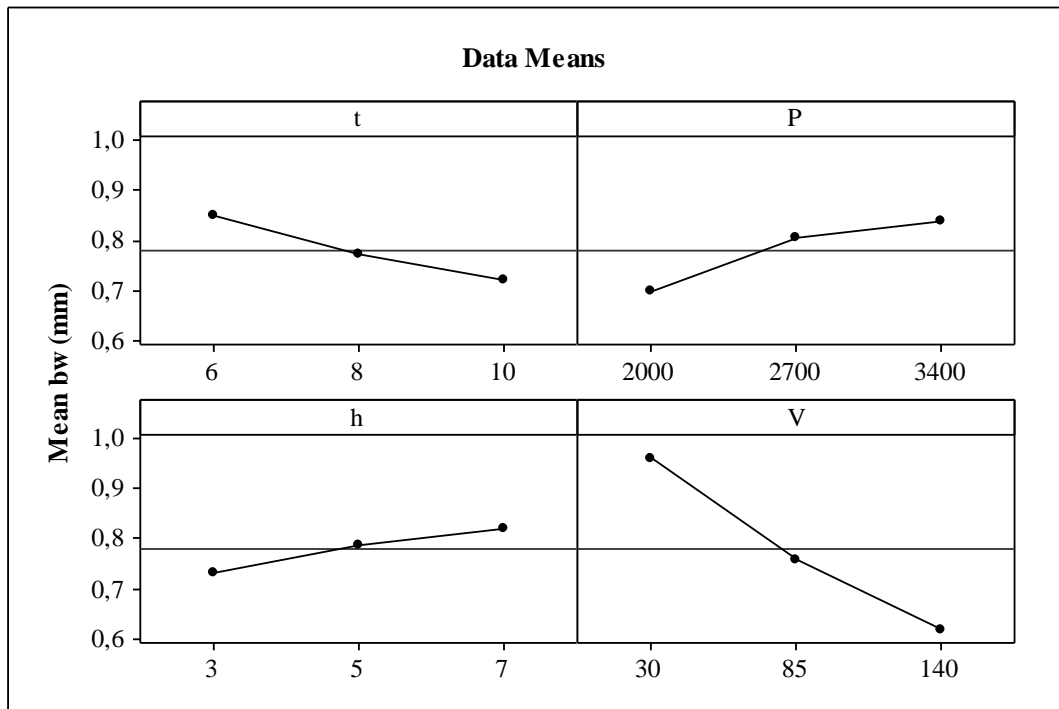
Figure 4.16 Main Effects of Process Parameters on Bottom Width (bw)

In Figure 4.17, main effects of process parameters into mean kerf taper angle (θ) is illustrated. From this figure, increasing of any of stand-off or traverse speed results as more tapered kerf geometry while the taper may reduce with an increasing in the waterjet pressure. Also it reduces with an increase in material thickness.
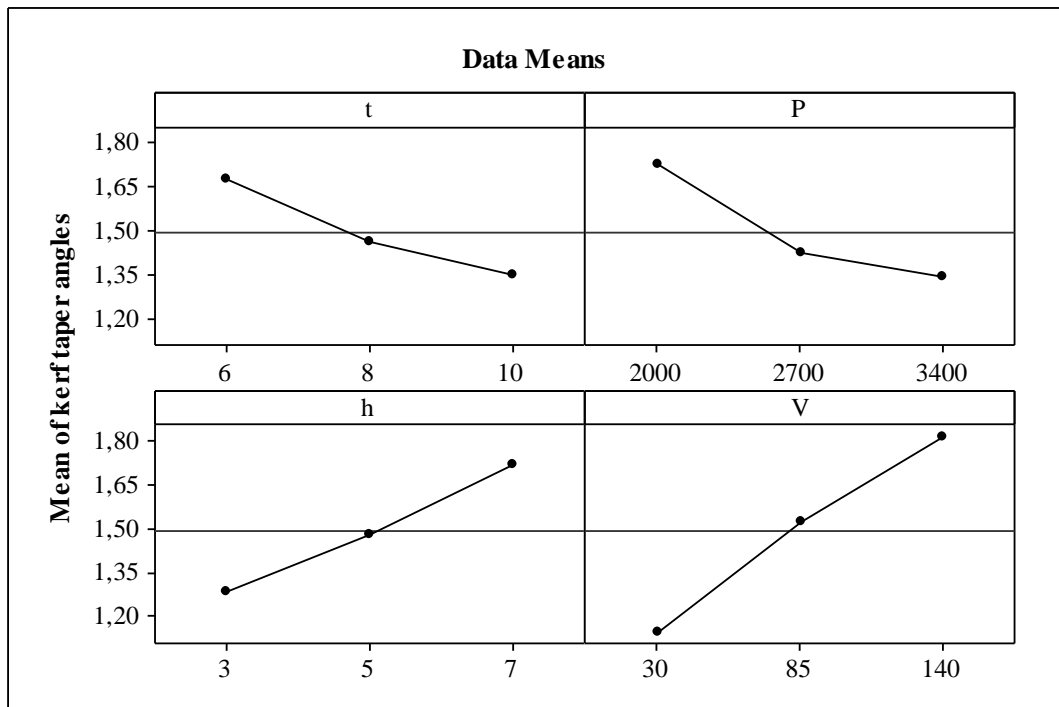
Figure 4.17 Main Effects of Process Parameters on Kerf Taper Angle (θ)

The behaviour of the process parameters into kerf taper angle is investigated in more detail by using interaction effect plot given in Figure 4.18. Increase in the traverse speed result in a decrease in the amount of the abrasive per unit time and this causes an increase in kerf taper angle. In addition to it, stand-off distance also increases the kerf taper angle. This is because the diameter of the jet enlarges with an increase in the stand-off distance.

On the other hand, this can be stated that the waterjet pressure creates a positive impact in kerf taper for each case. Kinetic energy of the jet increases with an increase in the waterjet pressure. This allows removing more pieces along the path of jet. Therefore, bottom width diameter enlarges and this provides smaller kerf taper.
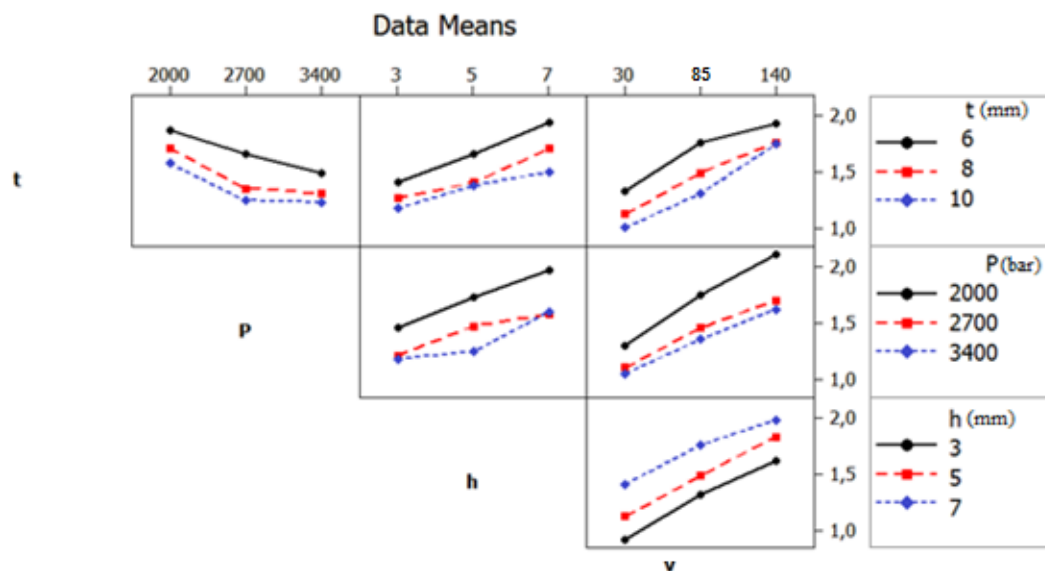
Figure 4.18 Interaction Effects of Process Parameters on Kerf Taper Angle (θ)

Finally, material thickness shows a positive impact on kerf formation. Increase in the material thickness results in a decrease in kerf taper.

CHAPTER 5

MODELLING

5.1   INTRODUCTION

A mathematical model is a description of a system using mathematical concepts and language. It may help to explain a system and to study the effects of different components, and to make predictions about behaviour. In any model, experimental data is used to fit the model by linear or nonlinear curves. Artificial neural network (ANN) and response surface methodology (RSM) are the two modelling methods that are commonly used for this purpose. In this chapter, experimental results are used for developing predictive models for surface roughness and kerf taper angle by using these modelling methods. For ANN models, back propagation network architecture with hyperbolic tangent sigmoid activation function is selected. In RSM model, both first order and second order equations are generated. Finally, they are compared to each other based on the statistical performance characteristics.

5.2   ARTIFICIAL NEURAL NETWORKS (ANN)

Artificial Neural Network is a mathematical model or computational model that is inspired by the neural structure of the human brain. A neural network consists of an interconnected group of artificial neurons, and it processes information using a connectionist approach to computation [37].

ANN is used in many applications such as pattern classification, clustering/categorization, function approximation, prediction and content addressable memory. Prediction, which will be the focus of this study, has a significant impact on decision-making in business, science and engineering.

5.2.1 Biological Neural Networks

Although how the human brain function is still a mystery, some aspects of this amazing processor are known. In particular, the most basic element of the human brain is a specific type of cell called neuron and it provides us our abilities to remember, think, and apply previous experiences to our every action. Each neuron has the same four basic components and these are known by their biological names - dendrites, soma, axon, and synapses. Dendrites, which are hair-like extensions of the soma act like input channels. These input channels receive their input through the synapses of other neurons. The soma then processes these incoming signals over time and turns that processed value into an output which is sent out to other neurons through the axon and the synapses. The representation of these components is given in Figure 5.1.
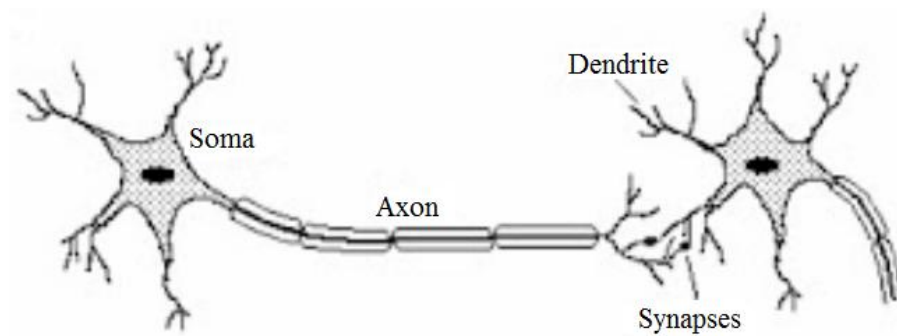
Figure 5.1 Representation of Biological Neurons [38]

5.2.2 Computational Models of Neurons

Among numerous neural network models that have been proposed over the years, all share a common building block known as a neuron and a networked interconnection structure. The most widely used neuron model is based on McCulloch and Pitts' work and is illustrated in Figure 5.2 [37].
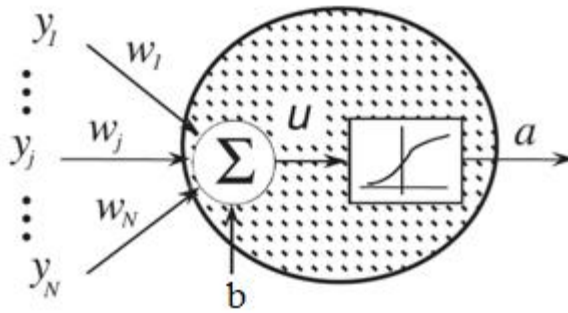
Figure 5.2 Mcculloch And Pitts' Neuron Model [37]

In Figure 5.2, each neuron consists of three main components, namely weights, bias and an activation function. Each neuron receives inputs (y_1, y_j,..., y_N) and then multiplied by the corresponding weight (w_1, w_j,..., w_N) which represents the connection strength for the input for each connection. Bias (b) is used to model the threshold is then added to summation of inputs and corresponding weighted linear combination is obtained in the following equation;

$$u_i = \sum_{j=1}^{N} w_j y_j + b \qquad (5.1)$$

The summation of u_i is then transferred using an activation function to yield a value called the unit's "activation", given as:

$$a = f(u) \qquad (5.2)$$

An activation function performs a mathematical operation on the signal output. In various neural network models, different activation functions have been proposed. The most commonly used activation functions are [39];

- Lineer transfer function;

$$a = purelin(u)$$

$$purelin(u) = u \qquad (5.3)$$

47
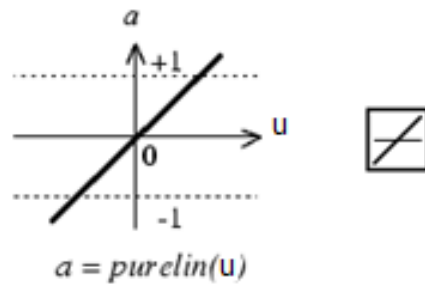
- Log-sigmoid transfer function;
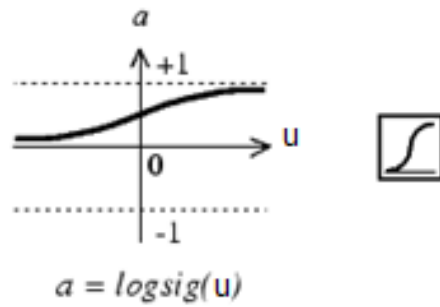
$$a = logsig(u)$$

$$logsig(u) = \frac{1}{1+e^{-u}} \qquad\qquad (5.4)$$

- Hyperbolic tangent sigmoid function
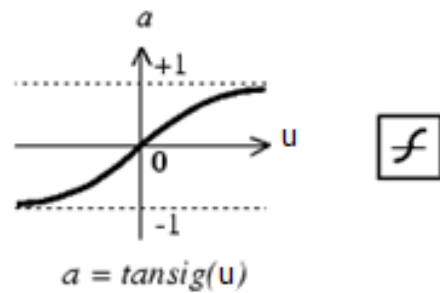
$$a = tansig(u)$$

$$\tan sig(u) = \frac{2}{1+e^{-2u}} - 1 = \tanh(u) \qquad\qquad (5.5)$$

The activation functions are chosen depending upon the type of the problem to be solved by the network. For example, if the network is desired to learn the average behaviour of a model, log-sigmoid function; if the average deviation is required to learn, hyperbolic tangent sigmoid function is recommended. In most of the studies they are determined by trial and error method.

5.2.3 Network Architectures

ANNs can be viewed as weighted directed graphs in which artificial neurons are nodes and directed edges (with weights) are connections between neuron outputs and neuron inputs.

Based on the connection architecture, ANNs can be grouped into two categories (Figure 5.3):

- Feed-forward networks; in which graphs have no loops,

- Recurrent (or feedback) networks, in which loops occur because of feedback connections. [40]
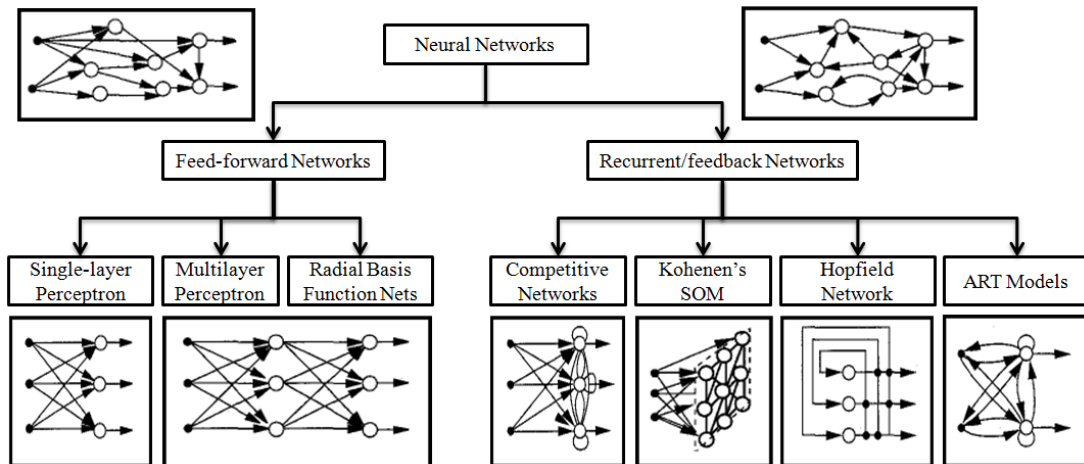
Figure 5.3 A Taxonomeny of Feed-Forward and Recurrent/Feedback Network Architecture [40]

5.2.4 Learning

The ability to learn is a fundamental function of intelligence. Although a precise definition of learning is difficult to formulate, a learning process in the ANN context can be viewed as the problem of updating network architecture and connection weights so that a network can efficiently perform a specific task. [40]

There are three main learning paradigms: supervised, unsupervised and hybrid. In supervised learning, or learning with a "teacher", the network is provided with a correct answer (output) for every input pattern. Weights are determined to allow the network to produce answers as close as possible to the known correct answers. In contrast, unsupervised learning, or learning without a teacher, does not require a correct answer associated with each input pattern in the training data set. It explores the underlying structure in the data or correlations between patterns in the data, and organizes patterns into categories from these correlations. Hybrid learning combines supervised and unsupervised learning. Part of the weights is usually determined

through supervised learning, while the others are obtained through unsupervised learning [40].

Table 5.1 Well Known Learning Algorithms [40]

Paradigm	Learning	Architecture	Learning	Task
Supervised	Error-correction	Single-multilayer perceptron	Perceptron learning algorithms	Pattern classification Function approximation
			Back-propagation	Prediction, control
	Boltzman	Recurrent	Boltman learning a.	Pattern classification
	Hebbian	Multilayer feed forward	Linear discriminant analysis	Data analysis Pattern classification
	Competitive	Competitive	Learning vector quantization	Within class categor. Data compression
		ART network	ARTMap	Pattern classification Within class categor.
Unsupervised	Error-correction	Multilayer feed forward	Sammon's projection	Data analysis
	Hebbian	Feed Forward or Competitive	Principal component analysis	Data analysis Data compression
	Competitive	Competitive	Vector quantization	Catg., data compress.
		Kohenen's SOM	Kohonen's SOM	Catg., data analysis
		ART networks	ART1, ART2	Categorization
Hybrid	Error-correction and competitive	RBF network	RBF learning algorithm	Pattern classification Function approx. Prediction, Control

5.2.5 Network Selection

Because all artificial neural networks are based on the concept of neurons, connections, and transfer functions, there is a similarity between the different structures, or architectures, of neural networks. The majority of the variations stems from the various learning rules and how those rules modify a network's typical topology (Table 5.2). Basically, most applications of neural networks fall into the following five categories [41]:

- prediction
- classification
- data association
- data conceptualization
- data filtering

Table 5.2 Network Selector Table [41]

Network type	Networks	Use for network
Prediction	Back propagation Delta bar Delta Extended delta bar delta Directed random search Higher order Neural Networks Self Organization Map into BP	Use input values to predict some output (e.g. pick the best stocks in the stock market, predict the weather, identify people with cancer risks)
Classification	Learning vector quantization Counter-propagation Probabilistic neural network	Use input values to determine the classification
Data association	Hopfield Boltzmann Machine Hamming network Bidirectional associative memory Spatio-temporal pattern recognition	Like classification but it also recognizes data that contains errors.
Data conceptual.	Adaptive resonance Self organizing map	Analysis the inputs so that grouping relationship can be inferred.
Data filtering	Recirculation	Smooth an input signal

5.2.6 Modelling With ANN

In this study, two separate prediction models for "Ra" and "θ" were developed by using ANN toolbox in "Matlab" software (R 2010a). Data set was randomly divided as 70%, 15% and 15% for training, validation and test data. Feed forward back propagation architecture with hyperbolic tangent sigmoid activation function (tansig) in both hidden layer and output layer was chosen in the creation of ANN. Networks consist of one input, one hidden and one output layer as illustrated in Figure 5.4. The training simulation was carried out using Levenberg-Marquardt back-propagation learning rule "trainlm" which is often the fastest backpropagation algorithm in the toolbox, and is highly recommended as a first-choice supervised algorithm [39].
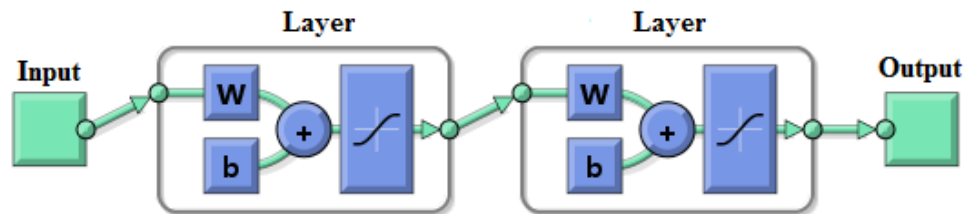
Figure 5.4 Network Architecture

During the training of the network many neuron numbers in the hidden layer are tested to find out the best results, namely highest correlation coefficient and minimum error rate. After trials the best results were obtained when there are 8 neurons in the hidden layer of surface roughness (Ra) model and 11 neurons in the hidden layer of kerf taper angle (θ) model. All the other training parameters for defined learning rule (trainlm) are taken the same as given in Table 5.3

Table 5.3 Training Parameters for Ra and θ Models.

Training Parameters	Description	Values
Show	Epochs between displays	25
Show window	Show training GUI	True
Show command Line	Generate command-line output	False
Epochs	Maximum number of epochs to train	1000
Time	Maximum time to train in seconds	Inf
Goal	Performance goal	0.001
Max_Fail	Maximum validation fails	6000
Mem_reduc	Factor to use for memory/speed tradeoff	1
Min_grad	Minimum performance gradient	1E-10
mu	Initial mu	1E-3
mu_dec	mu decrease factor	0.1
mu_inc	mu increase factor	10
mu_max	Maximum mu	1E10

The prediction of ANN and experimental values for training, cross validation, testing and all data are given in Figure 5.5 and 5.6 for Ra and θ model. Good agreement can be seen in these figures.
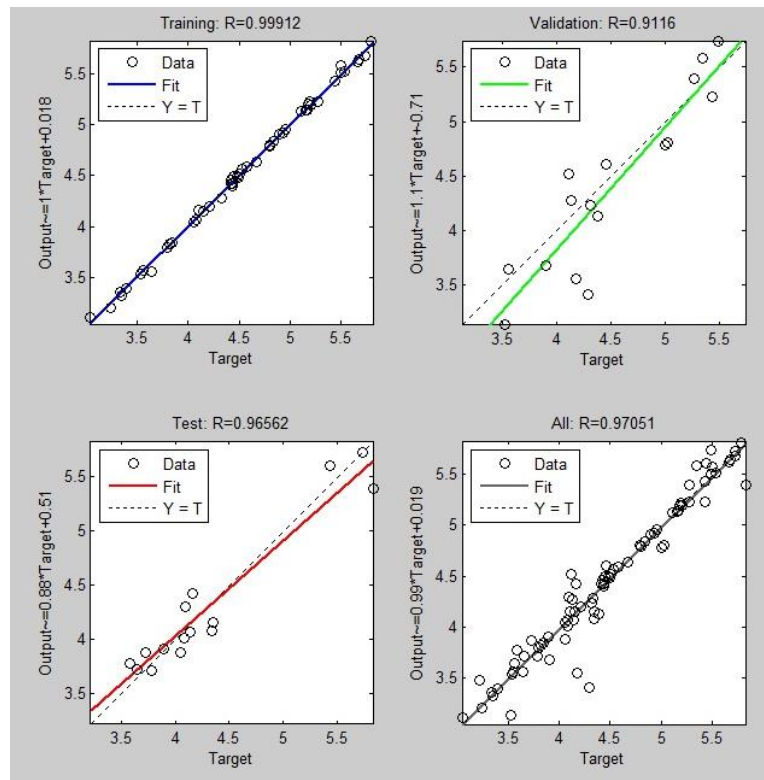
Figure 5.5 Regression Plots for Ra Model
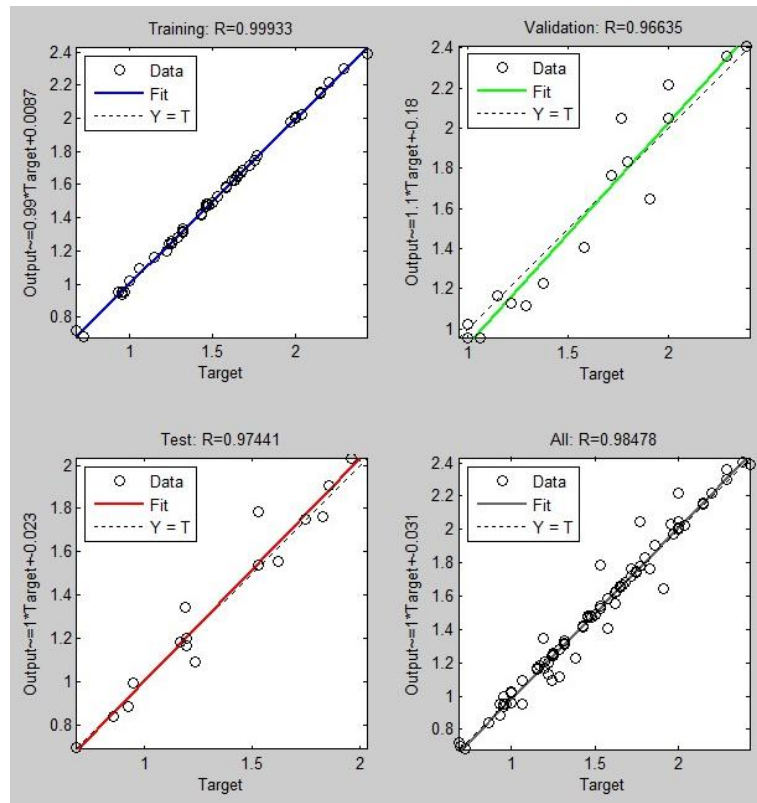
Figure 5.6 Regression Plots for θ Model

The values of weights and biases can be obtained from neural network toolbox for the models are given in Table 5.4 and 5.5 in an abbreviated form. In these tables, the terms represent:

iw{1,1} =Weight to layer 1 from input 1

Iw {2,1} =Weight to layer 1

b{1} =Bias to layer 1 (hidden layer)

b{2}= Bias to layer 2 (output layer)

Table 5.4 Weights and Biases for Ra Model

iw{1,1}	[-2.2541 -0.89941 -0.55929 0.73218; -0.2984 -0.13658 -0.47836 -0.10498;
	-3.0652 -0.49015 1.7081 -0.40614; -0.3313 -2.6552 0.57489 -2.7759;
	-3.6865 3.9958 0.14495 -4.1541; -0.10091 3.3917 1.0186 0.75179;
	0.99756 1.2531 0.12119 -0.50319; -0.61348 -0.19143 -2.999 -0.01527]
Iw{2,1}	[1.1754 -2.7993 -0.066503 -0.10949 -0.15281 0.14538 -0.71464 -
b{1}	[4.1752; 1.2212; 0.50239; -3.1687; -0.6122; 2.4205; 0.74445; -4.2738]
b{2}	[0.10866]

54

Table 5.5 Weights and Biases for θ Model

iw{1,1}	[-0.9357 -0.58655 1.357 1.829; 0.078466 -2.7603 0.22125 0.27017; -1.4681 -1.3265 2.39 -0.71027; 1.0072 1.1571 0.29359 1.6358; -1.1106 1.6813 1.9981 1.4185; -2.0547 0.89514 0.4164 -1.4317; -0.25915 -1.5109 2.605 -0.18903; -2.1967 -0.99916 0.31213 1.2109; 0.92118 -2.4098 -1.871 -1.0055; 1.7273 1.2578 0.78703 1.5065; -0.63572 -1.7308 0.30382 -2.7014]
Iw{2,1}	[1.2507 0.56012 -0.23488 0.2385 0.61859 0.19953 0.29914 0.15472 0.64607 -0.089681 -0.35392]
b{1}	[3.698; -2.8413; 0.54321; -1.6294; -1.0935; 0.16184; 0.35797; -1.4517; 1.583; 2.5848; -2.9125]
b{2}	[-0.88319]

5.3   RESPONSE SURFACE METHODOLOGY (RSM)

Response surface models are a kind of general linear model in which attention focuses on characteristics of the fit response function influenced by several independent variables. The aim is to find the relationship between the response and the variables. Therefore a model is used for developing the empirical equation based on the data. Here, order of the model is an important factor in how accurately the model describes the data and predicts a response. Depending on the approximation of the response function, either first order or second order models can be employed. The approximation function of first order (5.6) and second order (5.7) models can be expressed as:

$$y = \beta_0 + \sum_{i=1}^{k} \beta_i x_i + \varepsilon \tag{5.6}$$

$$y = \beta_0 + \sum_{i=1}^{k} \beta_i x_i + \sum_{i=1}^{k} \beta_{ii} x_i^2 + \sum \sum_{i<j} \beta_{ij} x_i x_j + \varepsilon \tag{5.7}$$

Where k is number of factors, β_0 is the free term, β_i is the linear effect, β_{ii} is the squared effect and β_{ij} is the interaction effect and ε is the experimental error. Second order model, also called quadratic or multiple-regression model, is used when there is a curvature in the response surface.

5.3.1 Modelling With RSM

In this study, both first order and second order mathematical models for Ra and θ are obtained in terms of the parameters (t, P, h, V) by using Minitab software. The analyses are performed using coded units and then they are transformed to uncoded units using the equation 5.8 to 5.11. Resulting estimated regression coefficients for coded units are given in Tables 5.6 and 5.7 for first order model; Tables 5.8 and 5.9 for second order model. Transformed response equations are summarized in Table 5.10.

$$x_1 = \frac{t - 8}{3} \qquad (5.8)$$

$$x_2 = \frac{P - 2700}{700} \qquad (5.9)$$

$$x_3 = \frac{h - 5}{2} \qquad (5.10)$$

$$x_4 = \frac{V - 85}{55} \qquad (5.11)$$

Table 5.6 Estimated Regression Coefficients for Ra

Term	Coef	SE Coef	T	P
Constant	4,49008	0,03343	134,306	0,000
Thickness (t)	0,05363	0,04095	1,310	0,194
Pressure (P)	-0,31060	0,04095	-7,586	0,000
Stand-off distance (h)	0,50401	0,04095	12,309	0,000
Traverse speed (V)	0,54968	0,04095	13,425	0,000
S = 0,300884 PRESS = 7,85975				
R-Sq = 83,73% R-Sq (pred) = 81,41% R-Sq (adj) = 82,87%				

Table 5.7 Estimated Regression Coefficients for θ

Term	Coef	SE Coef	T	P
Constant	1,4943	0,01729	86,452	0,000
Thickness (t)	-0,1619	0,02117	-7,646	0,000
Pressure (P)	-0,1904	0,02117	-8,993	0,000
Stand-off distance (h)	0,2174	0,02117	10,269	0,000
Traverse speed (V)	0,3320	0,02117	15,682	0,000
S = 0, 155568 PRESS = 2,08700				
R-Sq = 86,59% R-Sq (pred) = 84,78% R-Sq (adj) = 85,88%				

Table 5.8 Estimated Regression Coefficients for Ra

Term	Coef	SE Coef	T	P
Constant	4,71939	0,09439	50,000	0,000
Thickness (t)	0,05363	0,03853	1,392	0,169
Pressure (P)	0,31060	0,03853	-8,060	0,000
Stand-off distance (h)	0,50401	0,03853	13,080	0,000
Traverse speed (V)	0,54968	0,03853	14,265	0,000
t*t	-0,06643	0,06674	-0,995	0,323
P*P	-0,13093	0,06674	-1,962	0,054
h*h	-0,03314	0,06674	-0,496	0,621
V*V	-0,11348	0,06674	-1,700	0,094
t*P	0,10512	0,04719	2,227	0,029
t*h	-0,05943	0,04719	-1,259	0,212
t*V	0,05259	0,04719	1,114	0,269
P*h	0,02253	0,04719	0,477	0,635
P*V	-0,09043	0,04719	-1,916	0,060
h*V	0,01801	0,04719	0,382	0,704
S = 0,283161 PRESS = 8,03659				
R-Sq = 87,48% R-Sq (pred) = 80,99% R-Sq (adj) = 84,83%				

Table 5.9 Estimated Regression Coefficents for θ

Term	Coef	SE Coef	T	P
Constant	1,39850	0,04495	31,115	0,000
Thickness (t)	-0,16186	0,01835	-8,821	0,000
Pressure (P)	-0,19038	0,01835	-10,376	0,000
Stand-off distance (h)	0,21739	0,01835	11,848	0,000
Traverse speed (V)	0,33200	0,01835	18,093	0,000
t*t	0,05371	0,03178	1,690	0,096
P*P	0,11043	0,03178	3,475	0,001
h*h	0,01938	0,03178	0,610	0,544
V*V	-0,03975	0,02247	-1,251	0,215
t*P	0,00926	0,02247	0,412	0,682
t*h	-0,05192	0,02247	-2,310	0,024
t*V	0,03582	0,02247	1,594	0,116
P*h	-0,02315	0,02247	-1,030	0,307
P*V	-0,06004	0,02247	-2,672	0,009
h*V	-0,03221	0,02247	-1,433	0,157
S = 0,134838 PRESS = 1,79721				
R-Sq = 91,25% R-Sq (pred) = 86,90% R-Sq (adj) = 89,40%				

Table 5.10 Response Equations

First Order	
Ra =	3,36408 + 0,0268130 t - 0,000443712 P + 0,252004 h + 0,00999411 V
θ =	1,81956 – 0,0809323 t – 0,000271975 P + 0,108697 h + 0,00603635 V
Second Order	
Ra =	1,20490 + 0,123431 t + 0,000517710 P + 0,396353 h + 0,0180699 V - 0,0166065 t^2 - 0,000000267207 P^2 - 0,00828426 h^2 - 0,0000375127 V^2 + 0,0000750873 tP - 0,0148583 th + 0,000478131 tV + 0,0000160913 Ph - 0,00000234892 PV + 0,000163687 hV
θ =	3,39161 – 0,276403 t – 0,00132656 P + 0,233610 h + 0,0113398 V + 0,0134271 t^2 + 0,000000225358 P^2 + 0,00484558 h^2 – 0,0000131411 V^2 + 0,00000661206 tP – 0,0129790 th + 0,000325643 tV – 0,0000165368 Ph – 0,00000155951 PV – 0,000292792 hV

The analysis of variance (ANOVA) for regression analysis is given in Tables 5.11 and 5.12. For surface roughness (Ra) model, P value shows that the model, linear terms and squared terms are significant at the confidence level of 95% (α=0.05), however, interaction terms seem to have less significant effect. On the other hand, Table 5.12 shows that, all terms have significant influences on kerf taper angle (θ) for the same confidence level. Finally it can be concluded that all the linear, square and interaction effects should be considered in the prediction model of θ, while the interaction effects may be negligible in the prediction model for surface roughness.

Table 5.11 Analysis of Variance (ANOVA) for Ra

Source	DF	Seq SS	Adj SS	Adj MS	F	P
Regression	14	36,9862	36,9862	2,64187	32,95	0,000
Lineer	4	35,3978	35,3978	8,84944	110,37	0,000
Square	4	0,6395	0,6395	0,15989	1,99	0,106
Interaction	6	0,9489	0,9489	0,15815	1,97	0,082
Residual	66	5,2919	5,2919	0,08018		
Total	80	42,2781				

Table 5.12 Analysis of Variance (ANOVA) for θ

Source	DF	Seq SS	Adj SS	Adj MS	F	P
Regression	14	12,5155	12,5155	0,89397	49,17	0,000
Lineer	4	11,8762	11,8762	2,96904	163,30	0,000
Square	4	0,3066	0,3066	0,07665	4,22	0,004
Interaction	6	0,3327	0,3327	0,05545	3,05	0,011
Residual	66	1,2000	1,2000	0,01818		
Total	80	13,7155				

5.4   COMPARISON OF ANN AND RSM

In the previous sections ANN and RSM methods are explained and prediction models are generated by using these methods. In order to compare the estimation performance of the methods all the experimental data set is simulated in each model and they are statistically analysed. In Table 5.13 and 5.14 prediction values obtained in each model and experimental results are given together for surface roughness and kerf taper angle. It is seen in these tables that, predictive values are fairly close to experimental results. Therefore, these methods are said to be suitable for estimating surface roughness and kerf taper angle.

Table 5.13 Experimental and Predicted Results for Ra

No	Exp	ANN	FO	SO	No	Exp	ANN	FO	SO
1	3,2390	3,5175	3,6934	3,6271	42	5,1660	5,1220	5,0398	5,1556
2	4,2961	4,0510	4,2430	4,3101	43	4,0619	4,3074	4,4444	4,5091
3	4,4172	4,3424	4,7927	4,7661	44	5,1899	5,0431	4,9941	5,1903
4	4,3834	4,4497	4,1974	4,1831	45	5,3451	5,5402	5,5438	5,6445
5	5,1812	5,0724	4,7471	4,8841	46	3,3995	3,5785	3,1258	3,1635
6	5,4901	5,4124	5,2967	5,3582	47	3,6431	3,6400	3,6755	3,7182
7	5,0256	4,7979	4,7014	4,6729	48	4,1380	4,0714	4,2252	4,0459
8	5,2041	5,3642	5,2511	5,3919	49	3,8974	3,9065	3,6298	3,7051
9	5,6631	5,6443	5,8007	5,8839	50	4,3397	4,0783	4,1795	4,2779
10	3,5279	3,4707	3,3828	3,4102	51	4,5804	4,6985	4,7292	4,6236
11	4,0547	3,8800	3,9324	4,0028	52	4,1066	4,6306	4,1338	4,1805
12	4,1533	4,6963	4,4821	4,3684	53	4,7964	4,9211	4,6835	4,7713
13	3,8187	4,0638	3,8868	3,9888	54	5,7293	5,4238	5,2332	5,1350
14	4,8342	4,7052	4,4365	4,5993	55	3,3326	3,6423	3,8006	3,5378
15	5,8239	5,3914	4,9861	4,9829	56	4,1800	4,1784	4,3503	4,3259
16	4,0893	4,2995	4,3908	4,5011	57	5,1567	4,8233	4,9000	4,8872
17	5,2695	5,0457	4,9405	5,1296	58	3,9063	3,9806	4,3046	3,9749
18	5,4341	5,5997	5,4901	5,5313	59	4,4561	4,6515	4,8543	4,7811
19	3,0477	3,3148	3,0722	2,9315	60	4,8914	5,3435	5,4040	5,3604
20	3,3495	3,3936	3,6218	3,4336	61	4,4397	4,6628	4,8086	4,3459
21	3,5363	3,6358	4,1715	3,7087	62	5,5008	5,3585	5,3583	5,1700
22	3,6543	3,7165	3,5762	3,5326	63	5,7271	5,7228	5,9080	5,7673
23	3,7248	3,8743	4,1259	4,0527	64	3,5839	3,7775	3,4900	3,5311
24	4,1148	4,2688	4,6755	4,3459	65	4,1298	4,1517	4,0397	4,2289
25	4,3271	4,1557	4,0802	4,0674	66	4,5071	4,4241	4,5894	4,6997
26	4,5281	4,4226	4,6299	4,6055	67	4,3464	4,1527	3,9940	3,9908
27	4,9983	4,9061	5,1795	4,9167	68	4,6694	4,7851	4,5437	4,7066
28	3,7936	3,8566	3,7470	3,6489	69	5,4298	5,1189	5,0934	5,1954
29	4,4890	4,6314	4,2967	4,3844	70	4,7949	4,6205	4,4980	4,3843
30	5,5364	5,0275	4,8463	4,8931	71	5,4886	5,4815	5,0477	5,1180
31	4,2138	4,1869	4,2510	4,1455	72	5,7853	5,6805	5,5974	5,6248
32	5,1111	5,0032	4,8007	4,8991	73	3,2210	3,4833	3,1794	3,2626
33	5,4329	5,4522	5,3504	5,4257	74	4,0781	3,9665	3,7291	3,8699
34	4,4197	4,6470	4,7550	4,5758	75	4,4340	4,4088	4,2788	4,2503
35	5,2760	5,4044	5,3047	5,3474	76	3,5554	3,5023	3,6834	3,7449
36	5,6768	5,7044	5,8544	5,8920	77	4,3162	4,4505	4,2331	4,3702
37	3,5582	3,5155	3,4364	3,5371	78	4,4868	5,1914	4,7828	4,7685
38	4,0789	4,0159	3,9861	4,1822	79	3,7803	3,7156	4,1874	4,1608
39	4,4440	4,6950	4,5357	4,6004	80	4,9306	5,1224	4,7371	4,8041
40	3,8453	3,7990	3,9404	4,0562	81	4,9538	5,7095	5,2868	5,2205
41	4,1587	4,4231	4,4901	4,7194					

Table 5.14 Experimental and Predicted Results for θ

No	Exp	ANN	FO	SO	No	Exp	ANN	FO	SO
1	1,15	1,13	1,30	1,22	42	1,68	1,95	1,83	1,69
2	1,62	1,72	1,63	1,65	43	1,22	1,27	1,38	1,30
3	1,77	1,78	1,96	2,00	44	1,72	1,72	1,71	1,64
4	1,62	1,56	1,51	1,53	45	1,65	1,68	2,04	1,90
5	1,96	2,03	1,85	1,92	46	0,68	0,76	0,75	0,80
6	2,29	2,27	2,18	2,24	47	1,25	1,28	1,09	1,14
7	1,77	1,77	1,73	1,87	48	1,43	1,49	1,42	1,41
8	2,29	2,29	2,06	2,24	49	0,97	0,96	0,97	1,01
9	2,39	2,36	2,40	2,52	50	1,25	1,31	1,30	1,32
10	0,95	1,00	1,11	1,00	51	1,47	1,55	1,64	1,55
11	1,53	1,54	1,44	1,36	52	1,32	1,39	1,19	1,25
12	1,72	1,78	1,77	1,65	53	1,58	1,60	1,52	1,53
13	1,24	1,24	1,32	1,28	54	1,83	1,76	1,85	1,73
14	1,86	1,91	1,66	1,61	55	0,95	0,73	0,97	0,91
15	2,00	1,91	1,99	1,87	56	1,46	1,43	1,31	1,41
16	1,53	1,36	1,54	1,60	57	1,75	1,75	1,64	1,83
17	2,15	1,79	1,87	1,90	58	1,06	1,04	1,19	1,11
18	2,00	1,81	2,21	2,13	59	1,58	1,73	1,52	1,58
19	1,24	1,09	0,92	0,99	60	2,15	2,13	1,85	1,97
20	1,19	1,34	1,25	1,30	61	1,32	1,15	1,41	1,35
21	1,53	1,79	1,58	1,53	62	1,75	1,75	1,74	1,79
22	0,95	0,99	1,13	1,25	63	2,20	2,23	2,07	2,15
23	1,38	1,23	1,47	1,52	64	0,69	0,70	0,78	0,70
24	1,67	1,69	1,80	1,72	65	1,00	1,03	1,12	1,14
25	1,48	1,42	1,35	1,55	66	1,43	1,41	1,45	1,50
26	1,91	1,62	1,68	1,79	67	1,00	1,04	1,00	0,88
27	2,00	1,97	2,02	1,95	68	1,29	1,38	1,33	1,29
28	0,93	0,93	1,14	1,01	69	1,80	1,79	1,66	1,62
29	1,50	1,46	1,47	1,48	70	1,20	1,20	1,22	1,10
30	2,04	1,79	1,80	1,86	71	1,06	1,49	1,55	1,48
31	1,25	1,28	1,35	1,27	72	1,72	1,87	1,88	1,77
32	1,65	1,69	1,68	1,70	73	0,72	0,69	0,59	0,72
33	2,00	2,05	2,02	2,05	74	1,00	0,97	0,92	1,10
34	1,65	1,38	1,57	1,56	75	1,58	1,43	1,26	1,40
35	1,97	1,95	1,90	1,96	76	0,86	0,84	0,81	0,87
36	2,43	2,36	2,23	2,28	77	1,17	1,19	1,14	1,22
37	0,93	0,89	0,94	0,80	78	1,46	1,46	1,47	1,49
38	1,29	1,22	1,28	1,20	79	1,20	1,17	1,03	1,07
39	1,32	1,33	1,61	1,52	80	1,43	1,65	1,36	1,38
40	1,15	1,17	1,16	1,03	81	1,63	1,80	1,69	1,62
41	1,22	1,40	1,49	1,40					

In order to have detailed information about the prediction performance of the models, statistical parameters for each model is summarized in Table 5.15. It is found in the table that, the highest correlation coefficients and minimum error rates are obtained by using ANN models. This means that ANN model is more successful in estimating the outputs than the models used in RSM. If error rates are compared, it is seen that there is a small difference between the results obtained from ANN and second order RSM models. Considering the time required for constructing and training the network in order to obtain small error rates, second order RSM model is recommended. Because, in contrast to ANN model, generation of RSM model just take a couple of seconds. Also, it is seen in the table that, first order models have the worst statistical performance values. This is because, only linear terms are considered in this method, although square and interaction terms have significant effects on the outputs as illustrated in Table 5.11 and 5.12.

Table 5.15 Statistical Parameters of ANN and RSM Models

Parameters	ANN	FO	SO	ANN	FO	SO
Correlation Coefficient (R^2)	90,28%	83,73%	87,48%	91,57%	86,59%	91,26%
Sum of squared errors (SSE)	4,23	6,88	5,29	1,16	1,84	1,19
Mean of squared errors (MSE)	5,23%	8,49%	6,53%	1,44%	2,27%	1,48%
	Ra model			θ Model		

CHAPTER 6

DISCUSSIONS AND CONCLUSIONS

Waterjet (WJ) cutting is one of the most recently developed non-traditional manufacturing processes. It uses a fine nozzle to generate a coherent waterjet at a very high pressure (more than 4000 bar) and speed (approximately 3 mach). The impact of the water alone is enough to machine a material to a certain extent, however, with the addition of abrasive, the material removal rate in the process increases and almost every kind of materials have a thickness of 100 mm can be cut. Also, due to numerous advantages, such as versatility and no heat affected zone on cutting surface, it has become indispensable to today's manufacturing industry, especially automobile and aerospace. For this reason, the working principals and cutting process of this machine are aimed to investigate in detail in this study.

In order to be a competent on abrasive waterjet machine, many cutting operations are performed during this study for various materials. After these trials, surface quality and kerf taper angle were selected as two important performance parameters for describing the cutting quality and it was found that any change in the process parameters result in a decrease or an increase on them. Thickness of the material is also added to three major process parameters (waterjet pressure, traverse speed and stand-off distance) and a total of 81 cuts were undertaken based on full factorial design of experiment method in order to investigate the effects of each on cutting quality of Al 7075 alloy.

After cutting processes, measurements of surface roughness and kerf geometry (top and bottom width) are recorded. Main effects and interaction effects plots indicate the relationship between these parameters and outputs. Following conclusions are obtained:

- All the parameters considered are effective on both surface roughness and kerf taper angle. Only the effect of thickness of the material on surface roughness is so small that can be omitted.

- Increasing in thickness of the material results in lower kerf taper.

- The most effective parameters are found as traverse speed and stand-off distance. Increasing of any of them results in an increase in surface roughness and kerf taper angle.

- Pressure has a positive impact on surface quality and kerf taper. Increasing in the pressure results in a decrease of them.

- In order to have a good surface quality and low kerf taper, water pressure should be selected as high as possible while the other process parameters (traverse speed and stand-off distance) should be selected low for every thickness value of Al 7075 alloy between 6 mm to 10 mm.

Contribution of this study is two folds. First is the investigation of process parameters on cutting quality and second is the application of modelling methods (ANN and RSM) to the abrasive waterjet cutting process. Mathematical models are generated for the prediction of surface roughness and kerf geometry. Back-propagation network architecture with hyperbolic tangent sigmoid activation function is used for the prediction model of ANN. The network is then compared with the first order and second order RSM models. Results show that, both of these methods are suitable for estimating surface roughness and kerf taper angle with a small error range (below 10%). The best estimation is obtained with ANN network. However, the differences between the error rates of these methods are negligibly small and constructing and training the ANN network takes so much time. For this reason, in the modelling of surface roughness and kerf taper, second order RSM is recommended.

With the existing AWJ cutting machine, some other types of machining operations such as engraving and drilling may be studied and effects of cutting parameters on the cutting quality may be investigated. AWJ cutting study may be extended to turning operations by designing a new setup.

REFERENCES

[1]   Shanmugam, D.K. and Masood, S.H (2008). An investigation on kerf characteristics in abrasive waterjet cutting of layered composites, *J. Mater. Process Tech.*, **209**, 3887-3893.

[2]   Folkes, J., (2009). Waterjet-An innovative tool for manufacturing, *J. Mater. Process Tech.*, **209**, 6181–6189.

[3]   Turnxon Precision. http://www.turnxon.com/articles/articles_11.html

[4]   Wang, J. and Wong, W.C.K., (1998). A Study of Abrasive Waterjet Cutting of Metallic Coated Sheet Steels, *Int. J. Mach. Tools Manuf.*, **39**, 855-870.

[5]   Külekci, M.K. and Akkurt, A., (2001). Evolution of Quality of the Surfaces Produced by Abrasive Waterjet Cutting, *Niğde Ü. Müh. Bil. Der.*, **5-2**,13-24.

[6]   Akkurt, A., Kulekci M.K., Seker, U., Ercan, F., (2004). Effect of Feed Rate on Surface Roughness in Abrasive Waterjet Cutting Applications, *J. Mater. Process Tech.*, **147**, 389-396.

[7]   Çaydaş, U. and Hasçalık, A., (2007). A Study on Surface Roughness in Abrasive Waterjet Machining Process Using Artificial Neural Networks and Regression Analysis Method, *J. Mater. Process Tech.*, **202**, 574–582.

[8]   Karakurt, İ., Aydın, G., Aydıner, K., (2010). Effect of Cutting Parameters on the Surface Roughness of Granite in Abrasive Waterjet Cutting, *J. Earth Sci. App. Res. Centre of Hacettepe U.*, **32-2**, 99-110.

[9]   Shanmugam, D.K., Nguyen, T., Wang, J., (2008). Minimisation of Kerf Taper in Abrasive Waterjet Machining of Alumina Ceramics Using a Compensation Technique, *Int. J. Mach. Tools Manuf.*, **48**, 1527-1534.

[10]   Gudimetla, P., Wang, J., Wong, W., (2002). Kerf Formation Analysis in the Abrasive Waterjet Cutting of Industrial Ceramics, *J. Mater. Process Tech.*, **128**, 123-129.

[11]   Srinivasu, D.S. and Babu, R., (2007). A Neuro-Genetic Approach for Selection of Process Parameters in Abrasive Waterjet Cutting Considering Variation in Diameter of Focusing Nozzle, *J. Applied Soft Computing*, **8**, 809-819.

[12]   Davim, J.P., Gaitonde, V.N., Karnik, S.N., (2002). Investigations into the Effect of Cutting Conditions on Surface Roughness in Turning of Free Machining Steel by ANN models, *J. Mater. Process Tech.*, **205**, 16-23.

[13] Guzelbey, I.H., Cevik, A., Erklig, A., (2006). Prediction of Web Crippling Strength of Cold-Formed Steel Sheetings Using Neural Networks, *J. Const. Steel Res.*, **62**, 962-973.

[14] Kök, M., Kanca, E., Eyercioğlu, Ö., (2011). Prediction Of Surface Roughness In Abrasive Waterjet Machining of Particle Reinforced MMCs Using Genetic Expression Programming, *Int. J. Adv. Manuf. Technol.,* **55**, 955-968.

[15] Engineering Handbook. http://www.engineershandbook.com/MfgMethods/waterjet.htm, 26.05.2012

[16] Youssef, H.A., El-Hofy, H. 2008. Machining Technology. Machine Tools and Operations. 13:978-1-4200-4339-6. U.S.A: *CRC Press*.

[17] Flow International Corporation. Waterjet Seminar. Waterjet White Paper. (2002)

[18] Majet Su Jeti ile Kesme Sanayi, Biksan Sanayi Sit., Istanbul-TURKEY.

[19] Wardjet. http://www.wardjet.com/02-waterjet-relationship-parameters.html , 26.05.2012

[20] http://nptel.iitm.ac.in/courses/Webcourse-contents/IIT%20Kharagpur/Manuf%20Proc%20II/pdf/LM-37.pdf

[21] Qualjet, http://www.qualjet.com/Newsletter/Newsletter-20080115.htm

[22] Nevtaş Makine. http://www.nevtasmakine.com/ , 26.05.2012

[23] Yasser, M.A. and Wang, J. 2011. Machining With Abrasives - Chapter 9: Impact Abrasive Machining. New York, *Springer*.

[24] CMT Cutting Machine Tools Co., Ltd. http://www.ecvv.com/product/3224641.html, 27.05.2012

[25] Kennametal-Roctec Composite Carbide Abrasive Waterjet Nozzles: Product Catalog

[26] Wikipedia. http://en.wikipedia.org/wiki/Garnet, 12.02.2012

[27] Flow. http://www.flowwaterjet.com/en/ask-dr-hashish.aspx, 27.05.2012

[28] Akkurt, A., (2009). ASJ ile Kesilen AISI 1030 Çelik Malzemeden Elde Edilen Kesik Yüzey Özelliklerinin Diğer Kesme Yöntemleri ile Karşılaştırılması, *P.Ü. Müh. Bil. Der.*, **15**, 142-152.

[29] Kulekci, M.K., (2002). Processes and apparatus developments in industrial waterjet applications, *Int. J. Mach. Tools Manuf.*, **42**, 1297-1306.

[30]   Panigrahi, S.K.P. and Jayaganthan, R., (2011). Effect of Ageing on Microstructure and Mechanical Properties of Bulk, Cryorolled, and Room Temperature Rolled Al 7075 Alloy, *J. Alloys and Compounds*, **509**, 9609-9616.

[31]   Certified Inspection Report, certified number 478397, Alcoa (Birmingham, U.K.)

[32]   Industrial Mineral Co.(IMC), http://www.supremegarnet.com/specifications.htm, 12.01.2012

[33]   ISO Standarts, ISO 4287-4288.

[34]   Hasçalık, A., Çaydaş, U., Gürün H., (2007). Effect of traverse speed on abrasive waterjet machining of Ti–6Al–4V alloy, *J. Materials&Design*, **28**, 1953-1957.

[35]   Chen, L., Siores, E., Wong, W.C.K., (1996). Kerf Characteristics in Abrasive Waterjet Cutting of Ceramic Materials, *Int. J. Mach. Tools Manuf.*, **36-11**, 1201–1206.

[36]   Hashish, M. and Plessis, M.P., (1979). Prediction Equations Relating High Velocity Jet Cutting Performance to Standoff Distance and Multipasses, *J Eng Ind*, **101**, 311–318.

[37]   Yu Hen Hu, Hwang, J.N., (2002). Introduction to Neural Networks for Signal Processing. *CRC Press LLC*.

[38]   http://neuralfuzzy.blogspot.com/2008/05/biological-neuron-model-and-artificial.html

[39]   MATLAB User's Manual, Release R2010a.

[40]   Jain, A.K., Mao, J., Mohiuddin, K.M., (1996). Artificial Neural Networks: A Tutorial, Theme Feature. **18**, 31-44.

[41]   Anderson, D., McNeill, G., (1992). Artificial Neural Networks Technology, New York: *Kaman Sciences Co*.